Thesis

Anisotropy and Vortex State in the Quasi-Two-Dimensional Superconductor, α-(BEDT-TTF)$_2$NH$_4$Hg(SCN)$_4$

Hiromi Taniguchi

Department of Functional Molecular Science

School of Mathematical and Physical Science

The Graduate University for Advanced Studies

1996

Contents

1. *General introduction*

1.1 *Historical background of the vortex state in Type-II superconductor*

Since the first observation of superconductivity in mercury by Kamerlingh Onnes, the study of superconductivity have been developed with continuous interest. Up to now, many kinds of superconductors have been synthesized. One of them is the high-T_c cuprate superconductors, which were discovered by Bednorz and Muler in 1986.[1] Through the history of the study of superconductivity, the discovery of the high-T_c cuprates was one of the most remarkable events in the field of solid-state physics. Since then a lot of cuprate superconductors have been synthesized, such as $YBa_2Cu_3O_{7-\delta}$ (YBCO)[2] and $Bi_2Sr_2CaCu_2O_{8+\delta}$ (BSCCO),[3] and are classified into a kind of unconventional superconductors which have two types of peculiar features different from those of conventional superconductors. The one is about the mechanism of the occurrence of superconductivity. Through a large number of experimental and theoretical researches, it is a consensus to date that the high-T_c cuprate superconductors are the d-wave superconductors with a media of antiferromagnetic interaction to form the Cooper pair. It is needless to say that the conventional superconductors are s-wave superconductors based on the electron-phonon interaction, as predicted by BCS theory. The second, which is related to the main purpose of this thesis, is concerning the nature of the vortex state, namely superconductivity in magnetic fields. In the cuprate superconductors, which are extremely Type-II ones characterized by the relation of $\lambda >> \xi$ with penetration depth, λ, and coherence length, ξ, the behavior in fields was found to be quite different from that of the conventional Type-II superconductors. This

finding gave an opportunity to reconsider the vortex state. To clarify the difference between the conventional type-II superconductor and the unconventional one, first of all, the history of the former is surveyed below.

While the type-I superconductors have only the thermodynamic critical field, H_c, the type-II superconductors have two phenomenological critical fields for superconductivity. They are named lower critical field, H_{c1}, and upper critical field, H_{c2}. In the field-temperature (H-T) plane, $H_{c1}(T)$ and $H_{c2}(T)$ make an intermediate region between them in addition to the normal phase and the Meissner phase. This region is called mixed phase or Schubnikov phase (the vortex state, in this thesis). The theory concerning this phase was constructed by Abrikosov in 1957 with the mean-field approach and proved over several decades to describe accurately the phenomenological behaviors of the conventional superconductor. While the Meissner phase in $H<H_{c1}(T)$ is characterized by complete magnetic-field expulsion, in a mixed phase, $H_{c1}(T)<H<H_{c2}(T)$, the applied magnetic field penetrates the superconductor in a form of flux lines quantized in units of Φ, the flux quantum. The flux line consists of the normal core and the vortex of the supercurrent, of which the characteristic length scales are ξ and λ, respectively. And it was theoretically shown by Kleiner in 1964 that the assembly of them form a triangular lattice. Simultaneously, the dynamic property of the flux line was investigated theoretically by Bardeen and Stephen in 1965. When an external current density j is applied to the flux line system, the flux lines start to move due to the Lorentz force $F_L = j \times B/c$. If the system is perfectly clean, the driving force is counteracted only by the friction force $F\eta = -\eta v$, where η is viscous drag coefficient and v is steady-state velocity of the vortex system. Bardeen and Stephen modeled that the dissipation is

caused only by the movement of the normal core which have the normal state resistivity, ρ_n. And η was calculated and obtained as $\eta = BB_{c2}/c^2\rho_n$. So due to the motion of flux line, a finite electrical field appears in a superconductor, therefore the superconducting property of the dissipation-free supercurrent flow is lost. In this sense, an electrical resistivity in a mixed state is always finite, which is given by $\rho_f = \rho_n B/H_{c2}$, where ρ_f is flux flow resistivity. However, there must be disorders in real systems, and any disorder affecting superconducting order parameter contributes to a finite pinning force density, F_{pin}. Indeed, unless an applied current density exceeds a phenomenological critical current density, $j_c=cF_{pin}/B$, which makes the flux lines depin, electrical resistivity in mixed state is exactly zero except some special cases.

Next, the magnetic property will be described on the basis of the Been model, which is based on the concept of a constant critical current density, j_c, all over the superconducting volume. When a dc field is applied to a superconductor in the zero-field cooling condition, a inhomogeneity of the field distribution in the sample appears due to the pinning of flux lines. This pinning force is characterized by the critical current density $j_c=cF_{pin}/B$. In the field-increasing process, B linearly decrease from the surface to the center of the sample. The case of field-decreasing process is the contrary of the field-increasing process. So, these processes show the irreversible magnetization in the M–H curve, resulting in dissipation of magnetic energy. It is noted that any superconductor, as far as it has a finite critical current density, shows the irrversible magnetization.

Those are about the vortex state of the conventional superconductors. The important points are that the critical current density is finite and resistivity vanishes in

mixed state of simple conventional superconductor with real disorder.

In 1988, Palstra et al. measured electrical resistivity in the single crystal of BSCCO.[4] As seen in Fig.1-1, it was found that the transition curves is considerably broadened by the application of fields. Although transition curves in lower temperature side should enter into a region of the mixed state, the electrical resistivity remains finite. In this literature, this behavior was explained with a thermally activated flux flow (TAFF) model, which is based on the presence of the pinning centers which can permit the flux line to be depinned from them by thermal hopping. The simple version of this model is characterized by the formula of $\rho_f = \rho_n \exp(-U_0 / k_B T)$, where U_0 is the activation energy, which can be estimated by the relation of $U_0 = H_{c2} \xi a_0^2$ with a_0, a distance between neighboring flux lines. And the result was well explained with excellent quality of fitting, as shown in Fig.1-2. This fact suggests that in the high-T_c cuprates, the thermal activation of the flux-line motion can not be negligible because of high temperature and a small $\xi_{//}$, namely a small U_0. So flux lines tend to depin out of pinning centers, which may cause the finite resistivity in a wide range of mixed state.

Next, magnetic properties of the high-T_c cuprates are described. From the early stage of the study of them, the existence of what is called a irreversibility line, which separates a reversible region from irreversible region in H-T plane, is known. An example[5] about this feature is given in Fig. 1-3. Below $H_{c2}(T)$, there is a region where the magnetization is reversible in the M-H curves. This fact implies that, in a mixed state, there is characteristic region where j_c is zero or cannot be defined.

These resistive and magnetic features had been explained as extremely strengthened creep or thermally activated creep with a small activation energy. However,

it was shown later by a remarkable experiment that the vortex state of the high-T_c cuprates is essentially different from that of the conventional superconductors. In 1992, Safer et al. measured the resistivity of YBCO with high resolution of picovolt-order.[6] As shown in Fig.1-4, a clear resistive drop with hysteresis was observed, suggestive of a first-order phase transition. With predicted theories, it was considered as an evidence of a flux-line lattice melting. At present clearer data concerning this transition are reported in both YBCO[7] and BSCCO.[8][9] Figure 1-5 and Fig. 1-6 are the results of resistivity measurements of high quality single crystals of YBCO and BSCCO, respectively. Figure 1-7 shows a magnetization drop in the *M-H* curve, associated with the change of the flux-line density due to the melting. And recently a latent heat associated with this first-order transition was observed in the specific heat measurement,[10] as shown in Fig.1-8.

Through these experimental works, the flux-line lattice melting has been established in the high-T_c cuprate superconductors. Above this melting line in the *H-T* plane, the flux line should be in the liquid state. And this nature is considered to cause finite resistivity and zero critical currents in some region of mixed state. In this sense, the singularities of the vortex state of high-T_c cuprates originate in this melting transition, of which the mechanism will be explained in the next section.

1.2 *Fluctuations of vortices and instability of the Abrikosov lattice in Type-II superconductor*

The flux line lattice is, of course, a solid. There is the way to think that any solid melts into liquid when the followed relation holds.

$$\left\langle u^2 \right\rangle_{th} \cong c_L{}^2 a_0{}^2 \cdots\cdots\cdots\cdots (1-1) \ ,$$

where $<u^2>_{th}$ is a mean-squared thermal displacement, a_0 is a lattice constant and c_L is the Lindemann number, which is a constant value of 0.1～0.2. Such a melting scenario is called Lindemann criterion. When this criterion applies to the flux line lattice, $<u^2>_{th}$ means the mean-squared thermal fluctuation of displacement of flux lines and a_0 means the distance between neighboring flux lines, which is given by $1.07(\Phi/B)^{1/2}$ for the Abrikosov triangular lattice. Houghton et al.[11] calculated $<u^2>_{th}$ for an isotropic or anisotropic three-dimensional vortex system, and obtained following relation between $b_m(t)$ and t, where $b_m(t) = B_m(T)/H_{c2}(T)$, $t = T/T_c$.

$$\frac{\sqrt{b_m(t)}}{1-b_m(t)} \frac{t}{\sqrt{1-t}} \left[\frac{4(\sqrt{2}-1)}{\sqrt{1-b_m(t)}} + 1 \right] = \frac{2\pi c_L{}^2}{\sqrt{Gi}} \cdots\cdots (1-2) \ ,$$

where Gi is Ginzburg number, which will be discussed below, and is in a form of

$$Gi = \frac{1}{2}\left(\frac{k_B T_c \gamma}{H_c(0)\xi_{//}^{\ 3}}\right)^2 \cdots\cdots\cdots\cdots (1-3).$$

Here k_B is Bolzman constant , $\gamma = (m_\perp/m_{//})^{1/2}$ is anisotropic parameter and $\xi_{//}$ is in-plane coherence length. In a region near T_c and b_m<<1, the above equation can be simplified to

$$B_m(T) \approx 5.6\frac{c_L^{\ 4}}{Gi} H_{c2}(0)\left[1-\frac{T}{T_c}\right]^2 \cdots\cdots\cdots\cdots (1-4).$$

The experimental melting line in *H-T* plane in YBCO was well explained by this power-low relation, although the power coefficient is somewhat different from experimental value. The *Gi* measures the relative size of the minimum (T=0) condensation energy, $H_c(0)\xi_{//}^{\ 3}/\gamma$, within a coherence volume and critical temperature. And, in other words, it means the strength of the thermal fluctuations for a single vortex. While *Gi* amounts to an order of $10^{-8}\sim10^{-7}$ in conventional superconductors, *Gi* does to about 0.01 in YBCO, and becomes larger in BSCCO. These large *Gi*'s make the vortex lattice melting easy to be induced. Although the formula (1-4) is reformed in different regions in *H-T* plane, there is a general tendency that the melting line is qualitatively close to the H_{c2} line for a smaller *Gi*. Indeed, if this theory is applied to the vortex system of the conventional superconductor, the melting line is predicted to be considerably close to H_{c2} line with the difference of two lines indistinguishable.

Through the above discussion, the fluctuations of vortices, which can be measured by *Gi*, is found to be a important. A huge *Gi* causes the flux line melting. This feature may separate the unconventional superconductors from the conventional ones. It is important in the beginning of the vortex state study in any material to know the value of *Gi*.

1.3 *Vortex system in quasi-two-dimensional Type-II superconductor*

As mentioned in the previous section, one of the important ingredients to characterize the vortex state is found to be *Gi*. And such a discussion is mainly applied to the case of YBCO, which is an anisotropic but three-dimensional superconductor. However, BSCCO has a distinctive nature, which largely affects the vortex system. That is quasi-two-dimensionality, which is considered to complicate the *H-T* phase diagram further. In this section, in order to clarify the difference between the quasi-two-dimensional system and the anisotropic three-dimensional system in the superconducting state, first, the property of superconductivity under a field parallel to the conducting layers will be explained. In this configuration a qualitative difference between them is clear. As shown in the upper-left illustration of Fig. 1-9, in the anisotropic three-dimensional superconductor or the quasi-two-dimensional one near T_c, a flux line consists of a elliptical normal core enclosed with a vortex of supercurrent, reflecting the anisotropy of the system. When temperature is decreased and a relation of $T/T_c = [1-(\xi_{//}(0)/\gamma s)^2]^{1/2}$ holds in a layered superconductor, 3D-2D (from three-dimensional to two-dimensional) crossover occurs. Such a scenario was predicted in the Lawrence-Doniach formalism.[12] In this case, as shown in the lower-left illustration of Fig. 1-9, the concept of vortices changes. A normal core vanishes and flux quantum Φ is shut up in the rectangular region, $s \times \gamma s$, where s is a layer spacing. The γs is called Josephson length, which measures the relevant phase screening length where nonlinearity in the out-of-plane coupling are important. This is one of the parameters which measure the strength of out-of-plane correlation. On the other hand, the character

of the out-of-plane penetration depth, $\lambda_\perp$, also changes essentially between these two regimes. While $\lambda_\perp$ can be viewed as the London penetration depth with a larger effective mass $m_\perp$ in the 3D anisotropic case, in the quasi-2D case, $\lambda_\perp$ behaves as Josephson penetration depth, λ_J, which is given by a form of

$$\lambda_J = \left(\frac{c\Phi}{8\pi^2 s j_c}\right)^{\frac{1}{2}} \cdots\cdots\cdots\cdots (1-5) \ ,$$

where j_c is the maximum Josephson supercurrent density. When the system is seen as Josephson multi-layers, j_c may be represented by the Ambegaokar-Baratoff formula,[13)]

$$j_c = \frac{I_c}{S} = \frac{\pi}{2eSR_n}\Delta(T)\tanh\frac{\Delta(T)}{2k_BT} \cdots\cdots\cdots (1-6) \ ,$$

where I_c is the Josephson critical current, S is the area of the junction and Δ is the energy gap. The vortex made by parallel field in the quasi-2D system is called Josephson vortex. Its behavior is quite different from one if the usual vortex.

Through the above discussion, two characteristic lengths, $\wp s$ and λ_J are found to be meaningful in the quasi-2D system in place of $\xi_{//}$ and $\lambda_\perp$ in anisotropic 3D system. It is also noted that free energy function, which governs the vortex system, is also changed in form from the Ginzburg-Landau equation to the Lawrence-Doniach equation, as the dimensionality of the system is turned.

In such a quasi-2D system, the vortex state, which is made by application of magnetic field perpendicular to the conducting layers, is also quite different from that of

the 3D superconductors. An upper-right illustration in Fig. 1-9 shows the profile of a perpendicular flux line in the 3D system. The flux line consists of a cylindrical normal core enclosed with a cylindrical vortex. On the other hand, in quasi-2D case, as shown in a lower-right illustration, it is broken in the nonsuperconducting layers. In general, the disk-like unit of the in-plane vortex in called pancake vortex. When this system suffers thermal fluctuations, the new mode of the vortex motion appears. That is the out-of-plane tilt mode of the coupled pancake vortices, which can lead to breakdown of the out-of-plane coherence. If this mode is thermally induced, the out-of-plane resistivity ($I \perp$ conducting layers) may drastically change or suddenly appear with increasing temperature. This phenomenon is named thermally induced dimensional crossover or decoupling.

The pancake vortices are coupled through the Josephson energy and the electromagnetic one. These coupling energies are characterized by the Josephson length, γs, and in-plane penetration depth, $\lambda_{//}$, respectively. When an applied dc field is increased, both these lengths are overlapped with those of neighboring vortices and effective coupling energies become smaller. When the applied field becomes larger than both $\Phi / \gamma^2 s^2$ and $\Phi / \lambda_{//}^2$, pancake vortices become to feel less straightening force through the tilt modulus,C_{44} and tend to lose the out-of-plane positional order. This phenomenon is named field-induced dimensional crossover. In this way, the new concepts of field- or thermally induced dimensional crossover or decoupling of pancake vortices are introduced in the quasi-2D vortex system. The vortex state in BSCCO and BEDT-TTF molecule-based superconductor should be considered in this context, as will be discussed in the next section. Indeed, these two types of dimensional crossover were

predicted theoretically.[14)15)] Experimentally, in BSCCO, the field-induced one was reported in the magnetic measurement,[16)] neutron scattering[17)] and μSR experiment.[18)] As for the thermally induced decoupling, there has recently been a report in the local ac susceptibility measurement.[19)] Thus the dimensionality of the coupled pancake vortices starts to be extensively studied. Moreover, mechanism and profile of the melting line is also considered to be different in the quase-2D case. So the vortex state in the quase-2D superconductors is expected to be very complicated and is not yet fully characterized in the whole *H-T* plane.

1.4 *Organic superconductor and high-T_c superconductor*

Through the previous sections, it is found that there are two important ingredients which make the vortex state interesting. Those are the thermal fluctuations of vortices and the quasi-two-dimensionality. In addition to the high-T_c cuprates, BEDT-TTF (ET) molecule-based organic superconductors are prospective for the study of the vortex state in this sense. To serve the following discussion, the formula (1-3) is reformed as

$$Gi = \frac{1}{2}\left(\frac{k_B T_c \gamma}{H_c(0)\xi_{//}^{\ 3}}\right)^2 \propto \left(\frac{T_c \gamma \lambda_{//}(0)^2}{\xi_{//}(0)}\right) \cdots\cdots\cdots (1-7) \ .$$

Because Gi measures the size of fluctuations of vortices, the formula (1-7) means that high T_c, large γ, large $\lambda_{//}$ and small $\xi_{//}$ enhance the fluctuations of vortices. From this viewpoint, superconducting parameters of three typical Type-II superconductors are listed in Table 1-1,

Table 1-1. Superconducting parameters of three representative superconductors.[20]

parameter	YBCO	κ-ET	Nb
T_c(K)	92	9.5	9.5
$\xi_{//}$(Å)	16	60	380
$\lambda_{//}$(Å)	1400	8000	390
γ	5	200	1
Gi	0.01	10	5×10^{-7}

where YBCO, κ-(BEDT-TTF)$_2$Cu(NCS)$_2$ (κ-ET) and Nb are chosen as representatives of cuprates, organics and conventional superconductors, respectively. Both YBCO and κ-ET have much larger values of *Gi* than that of Nb. However, it is noted that the reasons why these superconductors have such large values are different between the two high-*Gi* superconductors. While *Gi* of YBCO is mainly enhanced by high T_c and small $\xi_{//}$, *Gi* in κ-ET is done by large $\lambda_{//}$ and large γ. This feature of κ-ET originates from the structure. Assuming that $\lambda_{//}$ is the London penetration depth, λ_L, $\lambda_{//}$ is given in terms of the carrier density, n, and the effective mass, m^* as

$$\lambda_{//}(0) = \sqrt{\frac{m^* c^2}{4\pi e^2 n}} \cdots\cdots\cdots\cdots (1-8) \quad .$$

Most of the ET-based superconductors have only a half hall per ET molecule. So carrier density is quite small. Therefore, $\lambda_{//}$ tends to be enhanced through the relation of (1-8). These materials have layered crystal structure, where conducting layers composed of ET are separated by thick insulating anion layers. So large γ is expected, reflecting this structural feature. Indeed, several experiments suggest that κ-ET is viewed as a Josephson-coupled system.[21)22)] In this way, *Gi* is enhanced by large $\lambda_{//}$ and γ in κ-ET, which seems to be common to the ET-based superconductors.

In conclusion in this section, ET-based superconductors, as well as BSCCO, have the two essential properties which make the vortex state interesting; that is the large fluctuations of vortices and the quasi-two-dimensionality of superconductivity.

1.5 *Organic superconductor,* α-(BEDT-TTF)$_2$NH$_4$Hg(SCN)$_4$, *and scope of the present study*

As discussed in the previous sections, the two key properties make the physics of the vortex state fertile and is found to be inherent in ET-based superconductors. For the study of the pancake vortices, the size of anisotropy is important, because Josephson length, γs, therefore, anisotropy parameter, γ, plays an important role of the out-of-plane correlation of the pancake vortices. The ET-based organics, which include a lot of superconductors with various values of anisotropy, γ, are quite available in the systematic research of this issue. The parameters of several organic superconductors are listed in Table 1-2.

Table 1-2. T_c and γ of several organic superconductors.[20)]

organic superconductor	T_c (roughly)	γ
κ-(MDT-TTF)$_2$AuI$_2$	4 K	10
β-(BEDT-TTF)$_2$IBr$_2$	2 K	?
κ-(BEDT-TTF)$_2$Cu[N(CN)$_2$]Br	10 K	<200
κ-(BEDT-TTF)$_2$Cu(NCS)$_2$	10 K	200
α-(BEDT-TTF)$_2$NH$_4$Hg(SCN)$_4$	1 K	? (>200)

As seen in the Table, anisotropy of the organic superconductor span a range between 10 and 200, or larger. Systematic studies of organics will lead to comprehensive understanding of the quasi-two-dimensional vortex system. In this thesis, α-(BEDT-

$TTF)_2NH_4Hg(SCN)_4$ (α-ET) is chosen among them. The α-ET is known as a quasi-two-dimensional layered metal with thick insulating anion layers. The superconducting transition temperature is reported to be around 1K.[23] The crystal structure of this material is shown in Fig.1-10 along with that of another layered system, κ-ET, and structural parameters of these materials are also listed in Table 1-3.

Table 1-3. Structural parameters[24] of α-ET and κ-ET.

Material	G	a [Å]	b [Å]	c [Å]	α [deg]	β [deg]	γ [deg]	V [Å^3]	Z
κ–ET	$P2_1$	16.241	8.448	13.136	----	110.32	----	1690.1	2
α–ET	P1	10.091	20.595	9.963	103.65	90.53	93.30	2008.1	2

Although there is structural difference between them, they have highly two-dimensional characters. As for κ-ET, the two-dimensional characters were already observed in the superconducting state, as mentioned in the above section. Roughly speaking, the thickness of insulating anion layer may be a measure of the size of anisotropy. The direction perpendicular to the conducting layers is a^* in κ-ET, that is b^* in α-ET. The layer period in the out-of-plane direction is about15Å for κ-ET and about 20Å for α-ET. So α-ET is expected to give higher anisotropy in the superconductivity than κ-ET. However, there is little experimental works on α-ET.

In the present work described in this thesis, the superconductivity in α-$(BEDT\text{-}TTF)_2NH_4Hg(SCN)_4$ was studied in the following two steps. The first one is characterization of anisotropy of the superconductivity in α-ET at a zero field through the measurements of sperconducting parameters such as λ, ξ and γ. The second is to

clarify the vortex state of α-ET.

This thesis is organized as follows: In Chapter 2, experimental method and techniques are described. The zero-field characterization of α-ET is described in Chapter 3, where extremely two-dimensional character of the superconductivity is revealed. In Chapter 4, the investigation of the vortex state in fields perpendicular to the layers is presented and the *H-T* phase diagram is discussed. Conclusion is given in Chapter 5.

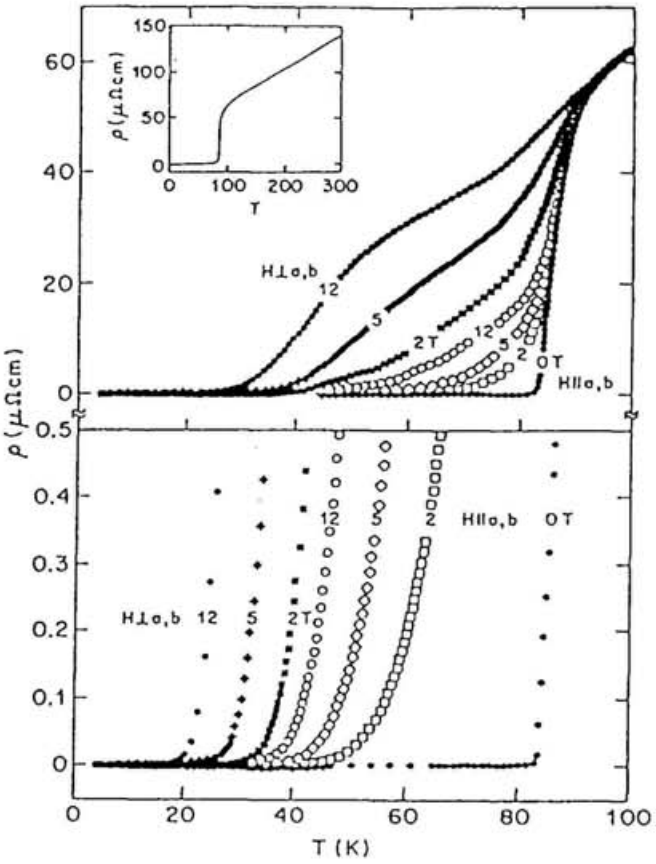

Fig. 1-1. Temperature dependences of resistivity of BSCCO in several magnetic fields.

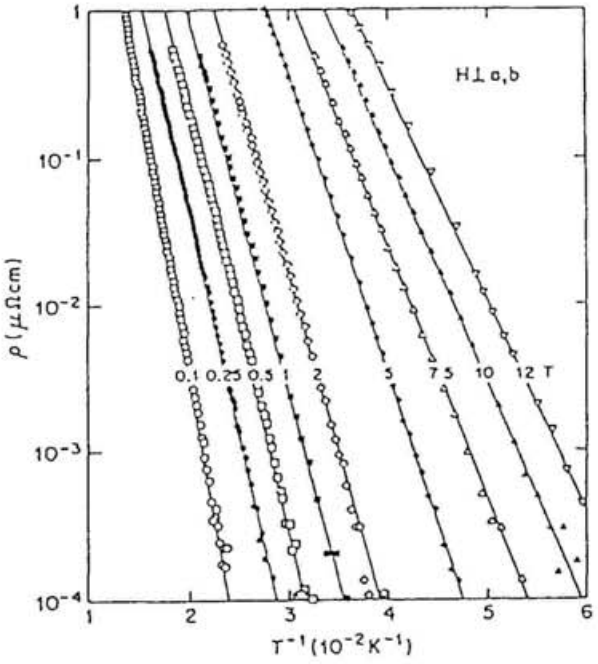

Fig. 1-2. Resistivities of BSCCO in activation-plot.

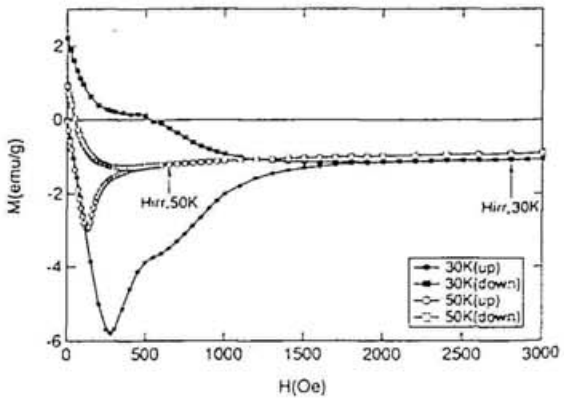

Fig. 1-3. Magnetization of BSCCO with irreversibility fields.

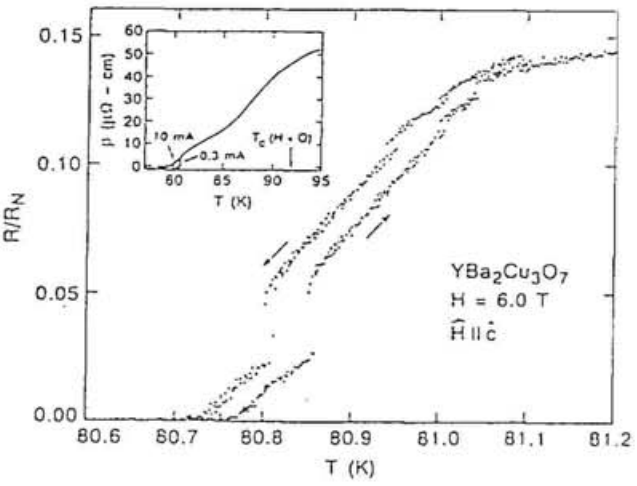

Fig. 1-4. Resistive drop of YBCO, suggestive of first-order transition.

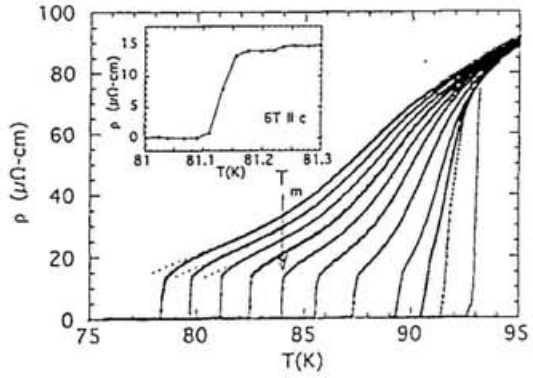

Fig. 1-5. First-order transition in resistive curves of YBCO.

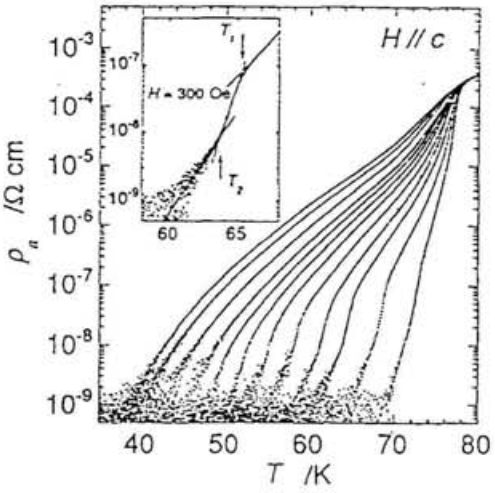

Fig. 1-6. Kink in resistive curves of BSCCO.

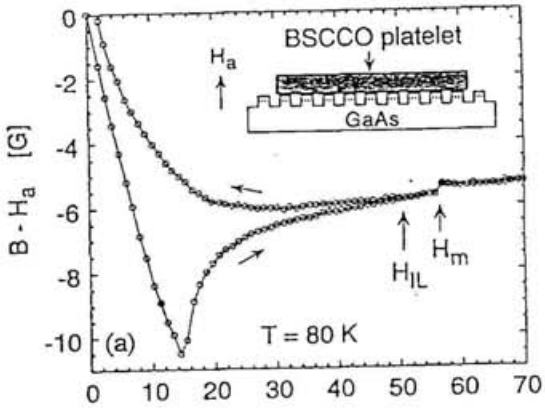

Fig. 1-7. Magnetic first-order transition in BSCCO.

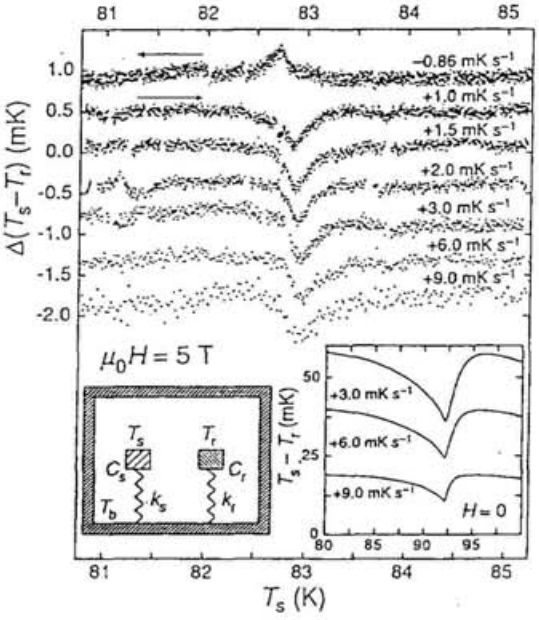

Fig. 1-8. Thermodynamic first-order transition in YBCO.

In case of anisotropic 3D

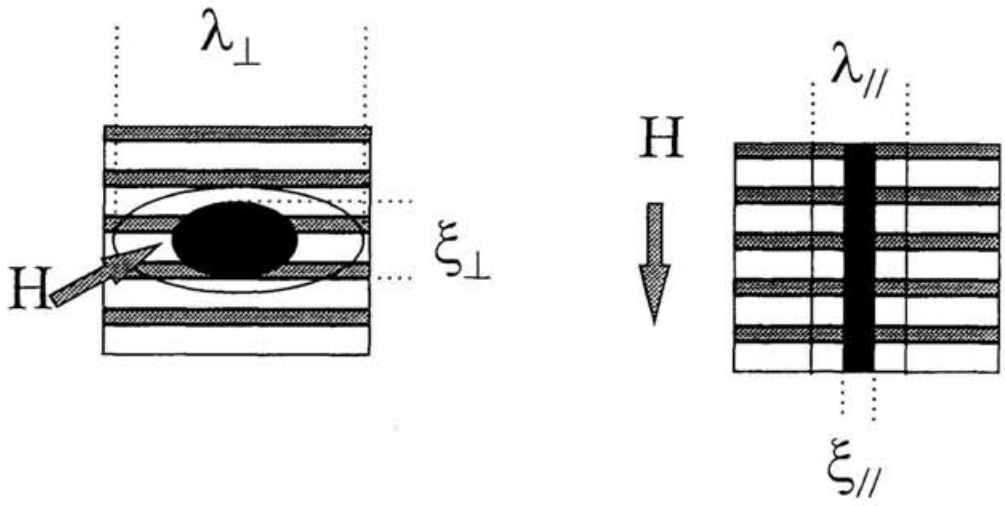

In case of quasi-2D

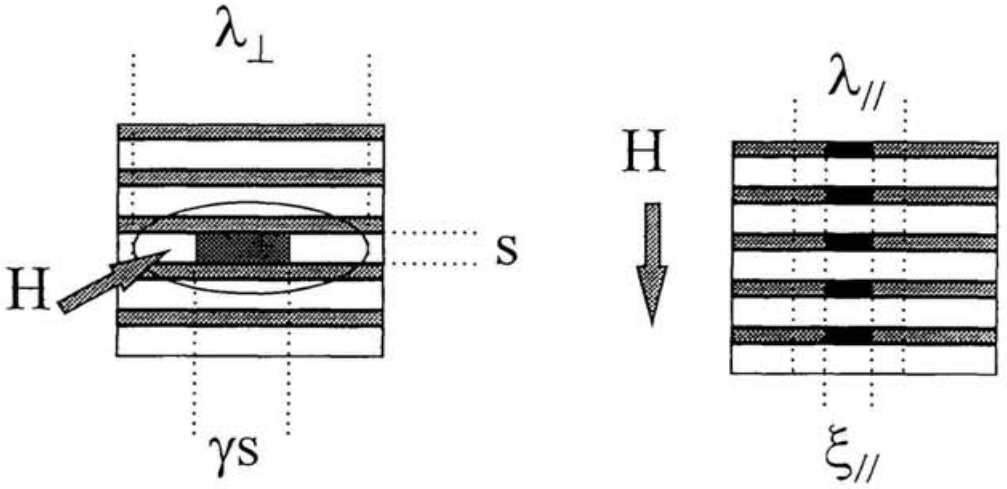

Fig. 1-9. Vortex systems in anisotropic-three-dimensional and quasi-two-dimensional superconductors.

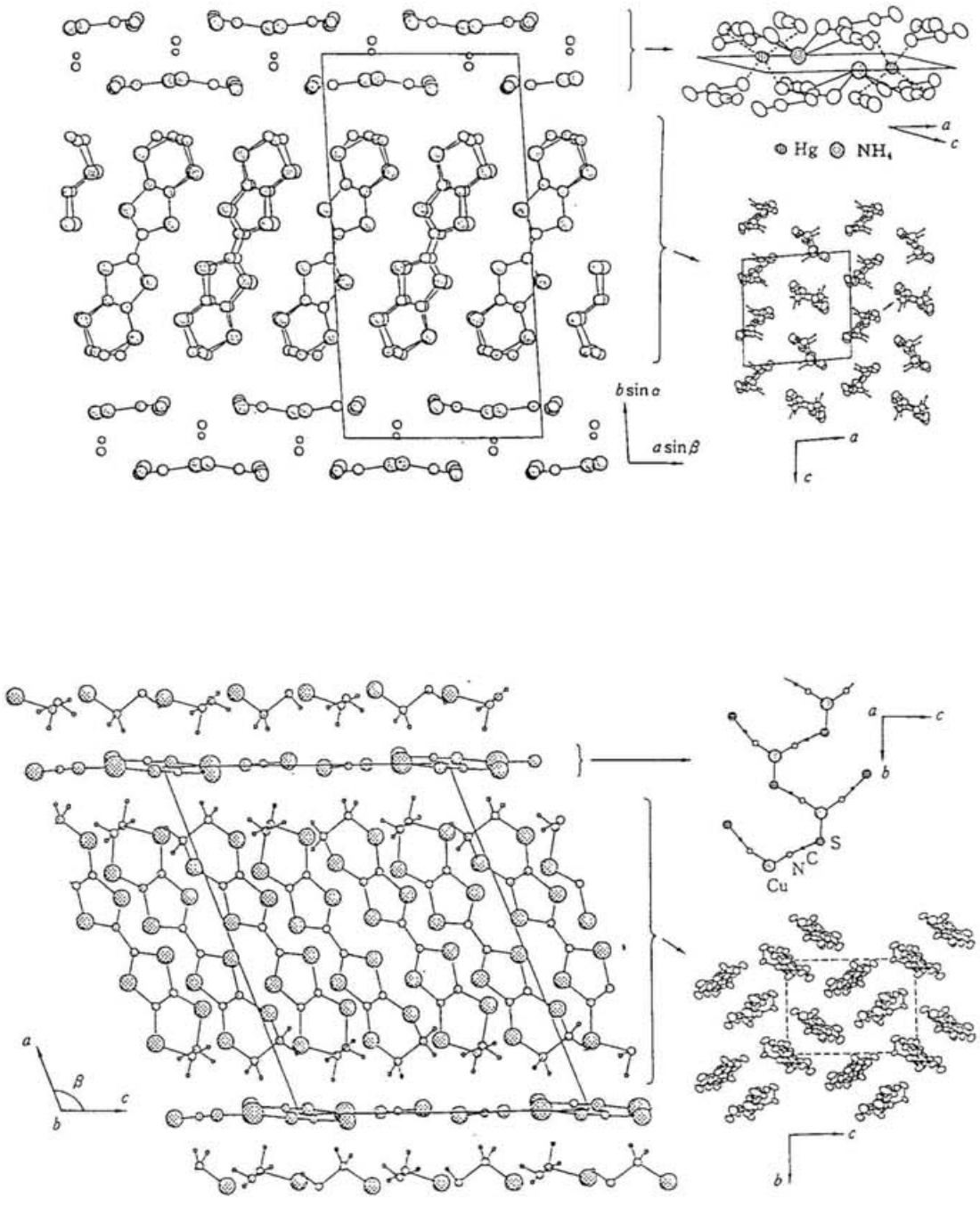

Fig. 1-10. Crystal structures of α-(BEDT-TTF)$_2$NH$_4$Hg(SCN)$_4$ (upper picture) and κ-(BEDT-TTF)$_2$Cu(NCS)$_2$(lower picture).

2. *Experimental*

2.1. *Sample preparation*

Single crystals of α-ET were grown[25] by the electrochemical method. BEDT-TTF (50mg), NH_4SCN (118mg), $Hg(SCN)_2$ (247mg) and 18-crown-6 ether (413mg), which were purified by recrystallization, were dissolved in a mixture of 1,1,2 trichloroethane (90ml) and ethanol (10ml). This solution was put in the glass cell under a argon-gas atmosphere. The glass cell has two platinum electrodes and a glass filter, as shown in Fig. 2-1. A constant current (1μA) was applied between the Pt electrodes under a condition of constant temperature (25℃), which was attained by a incubator. It usually takes 2-4 weeks to obtain single crystals with suitable size. Typical dimensions of single crystals selected for this work were $0.5\times0.5\times0.2\sim1\times3\times0.5$ mm^3.

2.2. *^{3}He refrigerator*

The superconducting transition temperature of α-ET is reported to be around 1 K.[23] The cooling below 1 K is required in the study of the superconducting state of α-ET. For this requirement, a ^{3}He refrigerator system was built. Figure 2-2 shows a diagram of a ^{3}He gas handling system. A volume of the ^{3}He gas is 4l at ambient pressure and temperature. In order to raise the performance on the lowest attainable temperature, a gate valve with diameter of 42 mm were used not to lose the evacuation conductance. To achieve the stability of temperature control of the system, a control valve with fine orifice was also used as a bypass line parallel to the gate valve line. A vellows tube with a diameter 60 mm connects the main gate and a cryostat to avoid vibrations due to a exercise of a rotary pump.

Figure 2-3 shows a detailed illustration of ^{3}He condensed room of the cryostat system. The lower part of a cryostat is surrounded by a vacuum insulation. So ^{3}He gas makes puddles in the bottom of this cryostat through the heat exchange on the Cu springs. The measurement platforms for ac susceptibility and resistivity is inserted into it so as to be soaked in liquid ^{3}He. The stability and agreement between temperatures at the thermometer and the sample are achieved in this condition. The lowest temperature achievable is 0.41 K and can be maintained for several hours, where the calibrated Cernox sensor is used as a thermometer in both the resistivity and ac susceptibility measurements.

2.3. *Magnetic field*

Even in the absence of applied field, a superconductor can be affected by the earth field (0.5 G). $H_{c1}(T)$ of α-ET is considered to be quite small as follows. H_{c1} is given in terms of λ and ξ as $H_{c1}=(\Phi / 4\pi\lambda^2)\ln(\lambda / \xi)$. λ and ξ will be given in the following Chapters. If these values are used, H_{c1} is about 8 G. This value is for perpendicular field. In parallel field, H_{c1} is much smaller. Thus, the effect of earth field on α-ET can not be negligible for the zero-field research. For this requirement, the measurements under a zero field were performed in the refrigerator surrounded by the double μ-metal shields. The residual dc fields was reduced to less than 1mOe or lower, which was confirmed by a Hall sensor.

The dc fields were applied with two types of superconducting magnet. The cryostat (^{3}He condensed system) was inserted to them as shown in Fig. 2-4. Resistivities and in-plane ac susceptibilities under fields were measured with the solenoid magnet-1, while out-of-plane susceptibilities were done with a split-type of magnet-2. Meanings and details of these measurements will be described in the following sections.

2.4. *Electrical resistivity measurements*

Electrical resistivity measurements were performed with four methods, which are illustrated in Fig. 2-5. The directions of the in-plane resistivity, $\rho_{//}$, and the out-of-plane resistivity, $\rho_{\perp}$, are also shown in Fig. 2-5. The configuration of leads are as follows.

(1) The four terminal method with four leads attached on the top surface of the crystal.

This method can characterize the in-plane resitivity, $\rho_{//}$, although the absolute value of it can not be determined.

(2) The four terminal method with two voltage leads attached on the top and two current ones attached on the edge surface of the crystal.

This can characterize the absolute value of $\rho_{//}$.

(3) The four terminal method with one current and voltage leads attached both surfaces of the crystal.

This can characterize the absolute value of out-of-plane resistivity, $\rho_{\perp}$.

(4) The six terminal method

This can characterize the both $\rho_{//}$ and $\rho_{\perp}$ without ambiguity of sample dependence, although the absolute value of $\rho_{//}$ can not be determined.

Hereafter these methods will be called as method-1, method-2, method-3 and method-4, respectively.

2.5. *ac susceptibility measurements*

Measurements of ac susceptibility were performed in the mutual inductance method in a temperature range of 1.4 K-0.4 K. The synthesized function generator, which has two source channels with a relative phase adjustable, was used as ac voltage sources; the first channel was used as the primary source which stimulate ac field, while the other was for the compensation of the off-valance signal above T_c (at 1.4K,usually). After the nulling adjust and phase setting were made by adjustment of voltage and phase of secondary channel of the function generator at about 1.4 K, temperature is decrease by pumping liquid ^{3}He. The diamagnetic signal of superconductivity was detected by a two-phase lock-in analyser as functions of temperature and applied dc magnetic fields. Sample temperature was monitored with a calibrated Cernox sensor down to 0.4 K. The apparatus was calibrated by two reference samples of conventional superconductors Cd (T_c=0.52 K) and Al (T_c=1.18 K). While ac field was always applied in the vertical direction, dc field was done in the vertical or horizontal direction. The samples were mounted so that the conducting layers were perpendicular or parallel to the direction of ac field, where dc field was perpendicular to the layers in each case. These configurations are shown in Fig. 2-4. In this thesis, the ac susceptibility in the former configuration is called the in-plane ac susceptibility, while that in the latter configuration is called the out-of-plane ac susceptibility. The reason will be described in the next chapter.

High-resolution ac susceptibility measurement was performed by a commercially available superconducting quantum interference magnetometer (Quantum Design ; MPMS2). Although the lowest temperature available is limited to 1.8 K, it was utilized to

pick up a very small ac response above the bulk transition temperature.

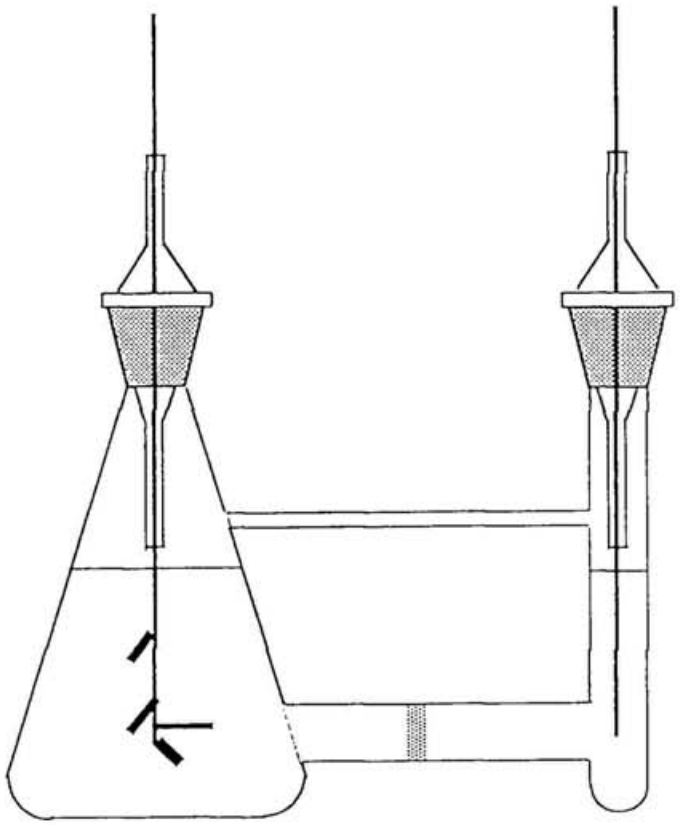

Fig. 2-1. Glass cell for growing single crystals.

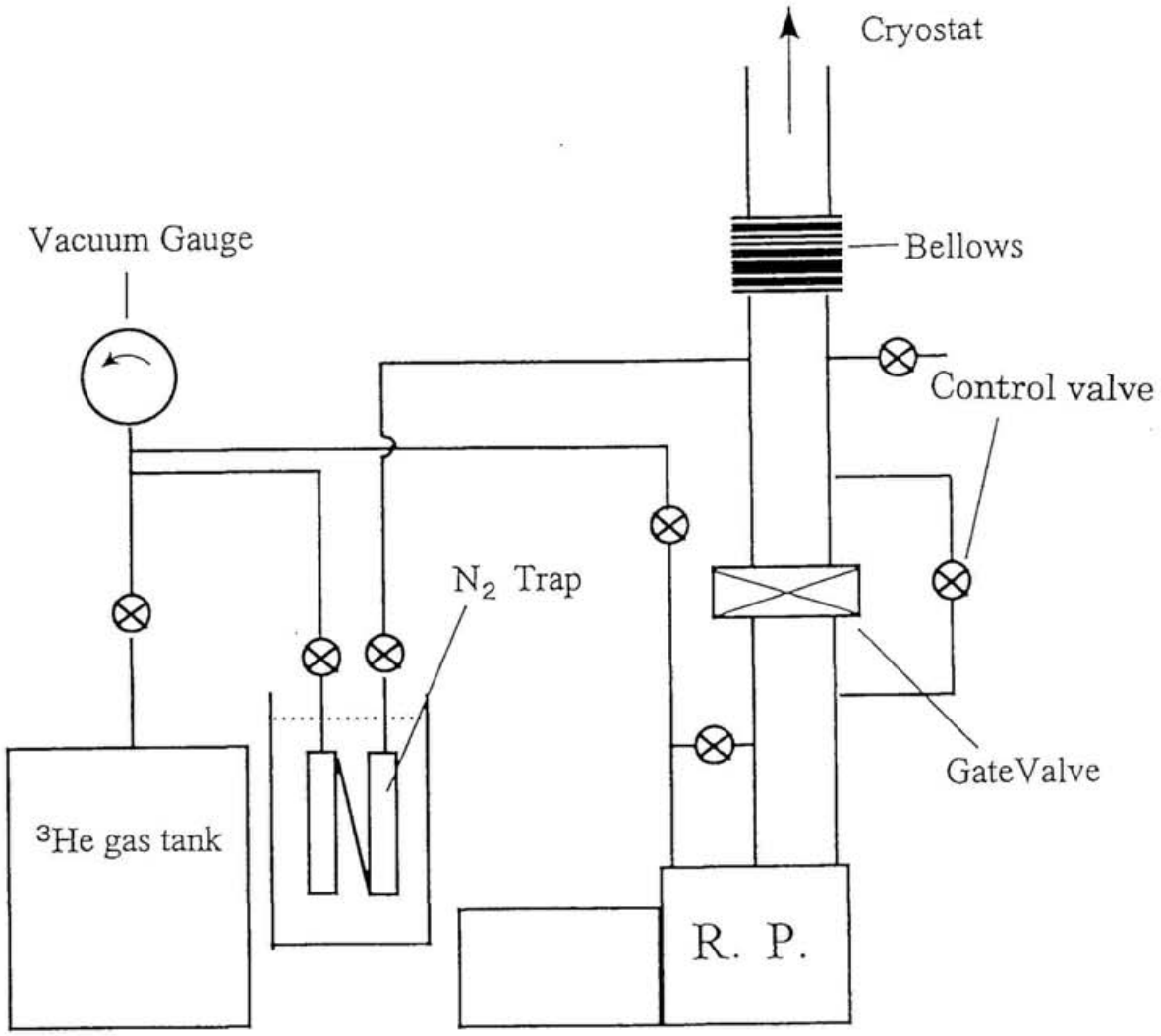

Fig. 2-2. ^{3}He gas handling system.

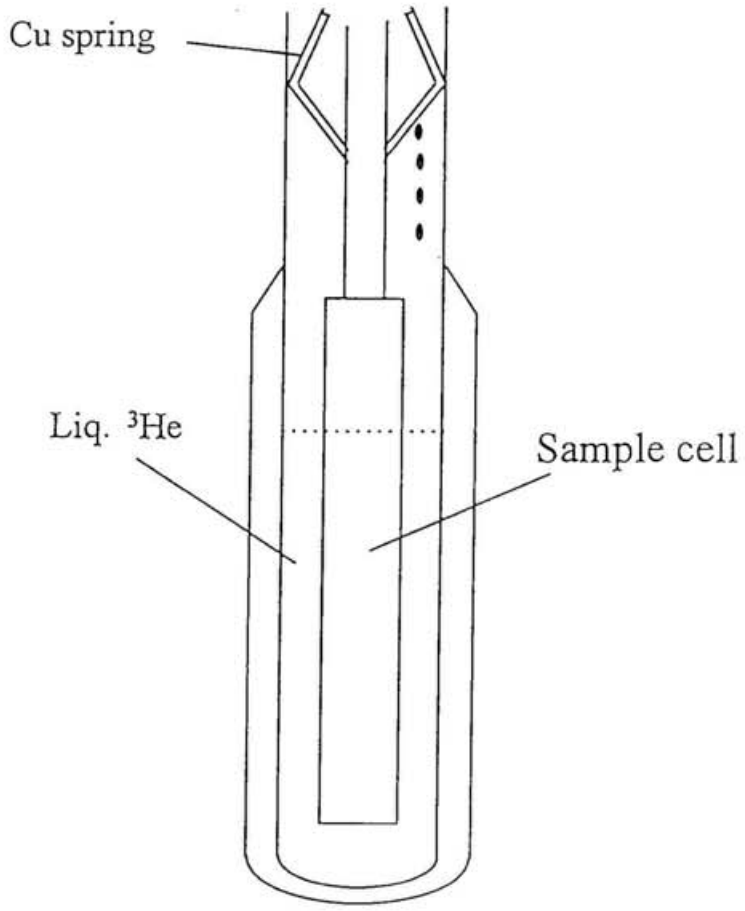

Fig. 2-3. ^{3}He condensation system.

Magnet-1

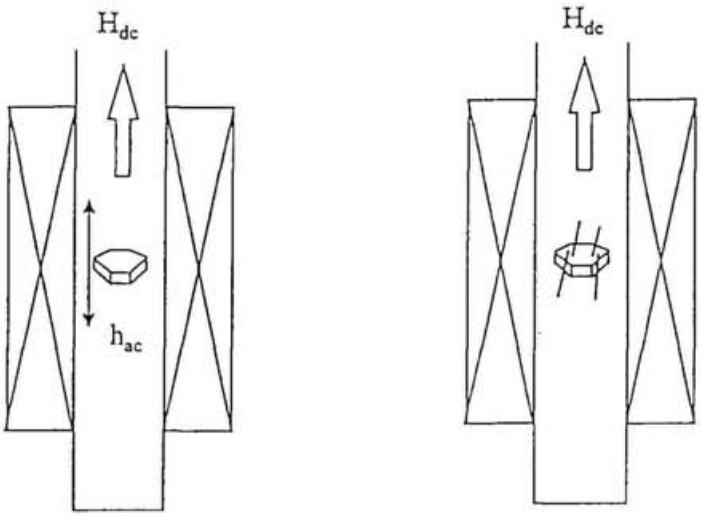

Magnet-2

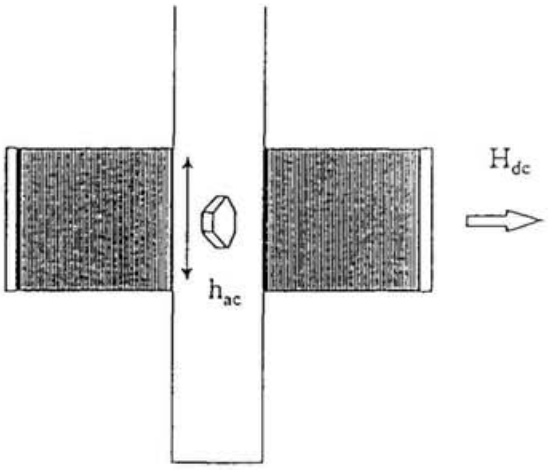

Fig. 2-4. Configuration of superconducting magnets and sample.

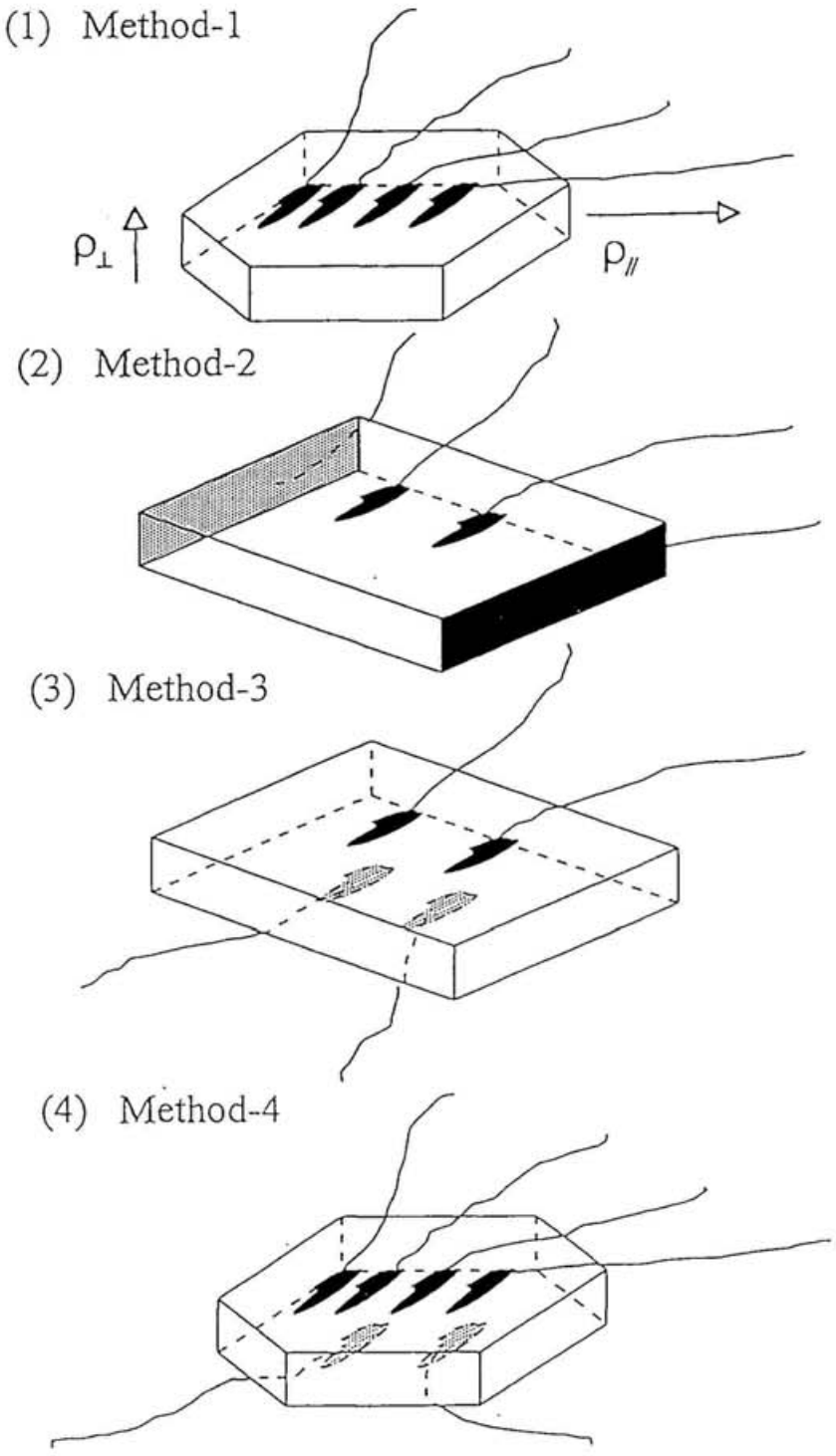

Fig. 2-5 Illustration of electrical terminal for measuring $\rho_{\perp}$ and $\rho_{//}$

3. *Superconducting characterization at a zero magnetic field*

3.1. Normal state property

α-(BEDT-TTF)$_2$NH$_4$Hg(SCN)$_4$ (α-ET) is a highly two-dimentional conductor. In such a material, the absolute value of the in-plane resistivity, $\rho_{//}$, is not easy to evaluate with reliable accuracy, while that of out-of-plane resistivity is obtainable by the method-3 or method-4, which are shown in Section 2.4. First, the absolute value of $\rho_{//}$ was examined by the method-2 in room temperature. Five crystals were examined and the obtained values were in a range of $1.5\times10^{-3}\sim3\times10^{-3}$ Ωcm and the average value of $\rho_{//}$ was 2 ± 0.5 mΩcm. On the other hand, the absolute value of out-of-plane resistivity was investigated through the method-3 or method-4. The number of crystals in this measurements amounts to 25.These results span a range of 400Ωcm～3000Ωcm. The averaged value was 1500 ± 500 Ωcm. If these values are used, the anisotropy of the resistivity, $\rho_{\perp}/\rho_{//}$, amounts to 7.5×10^{5}.

For the second method to evaluate $\rho_{\perp}/\rho_{//}$, a crystal which is the most symmetrical and has the nearly rectangular shape was chosen among all grown crystals. The $\rho_{//}$ and $\rho_{\perp}$ were examined for this identical crystal according to the method-4. The results were analyzed with the method which was applied to the single crystal of BSCCO by Bush et. al.[26] Although the details of the analysis is not mentioned here, this method is based on the determination of the inhomogeneous current distribution by solving the Laplace equation. In this way, $\rho_{//}$ and $\rho_{\perp}$ were obtained on an identical crystal. Application of this method to the present sample yielded the values of $\rho_{//}$=0.5mΩcm and $\rho_{\perp}$=1900Ωcm. This

result gave the anisotropy of $\rho_{\perp}/\rho_{//}=3.8\times10^{6}$.

Through the above two method, the anisotropy of resistivity was obtained as 7.5×10^{5} and 3.8×10^{6}. The difference may show the difficulty of the determination of the absolute value of the resistivity in such a highly anisotropic conductor. In any way, $\rho_{\perp}/\rho_{//}$, one of the important parameter, was concluded to be $\sim10^{6}$, which is used in the following discussions.

Next the temperature dependence of resistivity is presented. Fig.3-1 shows the temperature dependence of the in-plane resistivity, which are normalized to the value at 300K. These measurements were made by the method-1 or method-4. All the samples show metallic temperature-variation of resistivity in a whole temperature range below 300 K. The moderately negative curvature seems to be common to most of the crystals. Fig.3-2 shows the results of out-of-plane resistivity which was obtained as absolute value by the method-3 or method-4. In this configuration, $\rho_{\perp}$ shows metallic behavior as well as in-plane case and has clearer negative curvature than $\rho_{//}$. The temperature dependence is fairly well reproduced within the present crystals. [It is noted that a few samples show a broad maximum at 50-150K in both directions. This origin is unclear.] While resistivities in BSCCO[27] and κ-ET[28] are known to have complicated temperature dependence with the different behavior in different direction, α-ET seems to have nothing anomalous in spite of extremely two dimensional nature.

3.2 *Transport property in the superconducting state*

Under a zero magnetic field attained by the double-μ metal shields, the resistivity was measured with the six terminal method (method-4 in Section 2.3) in the superconducting state. This aims at investigating the anisotropic behavior without ambiguities of sample dependence. In this configuration for such a highly anisotropic metal, one does not obtain the absolute value of the in-plane resistivity, $\rho_{//}$. So $\rho_{//}$ is normalized to the value at 4K, while the absolute values of the out-of-plane resitivity, $\rho_{\perp}$, is obtained. The results for three crystals are shown in Fig. 3-3. The profile of the resistive transition was qualitatively different in the in-plane and out-of-plane measurements. The in-plane resistivity starts to decrease around 2.4 K with a tail of positive curvature and vanishes around 1K. On the other hand, the out-of plane resistivity exhibits a comparatively sharp transition around 1 K with negative curvature. This suggests that, in the temperature range from 2.4 K down to 1.0 K, the superconducting coherence starts to grow gradually within the layers but does not between the layers. This characteristic will be discussed in Section 3.4 along with the susceptibility data. It is noted that these behaviors are almost reproduced with good agreement of absolute values of $\rho_{\perp}$ for the present three crystals.

3.3. *ac-susceptibility in the superconducting state*

The ac-susceptibility, $\chi = \chi' - i\chi''$, was also measured under a zero dc field in a temperature range of 0.4-1.5 K. The ac field was applied perpendicular or parallel to the conducting layers. The former configuration gives in-plane susceptibility because a shielding ac current flows only in the in-plane in a sample, while the latter gives out-of-plane susceptibility because of induce of out-of-plane shielding current as well as in-plane one, which turns out not to be important in the present study of a highly anisotropic superconductor described later. Figure 3-4 shows in-plane ac-susceptibility under an ac field of 47 Hz and 0.16 Oe (in amplitude), which is confirmed to be in the low frequency and low amplitude limit from the frequency and amplitude dependence of the susceptibility. A sharp transition in χ' with an onset around 0.95 K appears and is followed by the saturation below 0.8 K. This indicates that the bulky coherence is established below 0.95 K, which is consistent with the specific heat results.[29] The saturation value of $4\pi\chi'$ is 2.8 times as large as the complete diamagnetism due to a large demagnetizing effect in the present geometry of the field and a specific shape of the crystal used. Rough estimation of the demagnetizating factor ensures that the saturation value corresponds to the perfect diamagnetism. Above 1.0 K, $-4\pi\chi'$ is smaller than a level of 10^{-2}, which is a resolution of our inductive apparatus under the present condition of the low frequency, low amplitude, and crystal size. More sensitive measurements in this high temperature range will be presented in Section 3.4.

The out-of-plane susceptibility measured by the inductive method is shown in Fig.3-5. In this geometry, the demagnetization effect is not significant. (This is also

because the susceptibility value is much smaller than unity as seen below.) So the absolute values of χ' and χ'' are obtained. The applied ac field is 0.16 Oe in amplitude and 1007 Hz in frequency. The onset of the transition is at 0.95 K, which coincides with that of the in-plane susceptibility. A strong contrast to the in-plane case is that $-4\pi\chi$' increases gradually with decreasing temperature and reaches only 20 % of the perfect diamagnetism at the lowest temperature available. This fact suggests that the penetration depth is comparable with the sample size. This feature can not be seen in the isotropic materials or weekly anisotropic ones. This will be discussed in Section 3.5 in terms of the absolute value of penetration depth in this geometry.

3.4. *In-plane characteristics and two-dimensional fluctuation; quasisuperconducting state above 1 K*

In order to examine the diamagnetic response in the in-plane configuration with higher sensitivity in a higher temperature range, where the in-plane resistance shows an appreciable and gradual decrease, a commercially available superconducting quantum interference device magnetometer was utilized for picking up very small ac response, although the lowest temperature available is limited to 1.8 K. A very small (less than 10^{-3}) but clear in-plane diamagnetic response was observed below $\sim$2.5 K, and was found to decrease by applied dc fields, as shown in Fig.3-6. This signal was confirmed to be independent on frequency of the ac field in a range from 1 to 10^3 Hz. Therefore, the diamagnetic signal is due to the superconductivity. As for the out-of-plane geometry, no diamagnetic signal was observed within this high sensitivity in this temperature range. This is consistent with the behavior of the out-of-plane resistivity and again indicates that the growth of the superconductive coherence is confined within the layer above 1 K. The behavior above 1 K can be considered to come from two-dimensional fluctuations of order parameter or inhomogeneity with slight admixture of high T_c inclusion. The good reproducibility of the resistive transition profiles and the smooth transition curves, which is shown in Fig. 3-3, seem to suggest that some intrinsic effect different from the inhomogeneity is involved in this quasisuperconducting behavior above 1 K. Some samples show in-plane current-voltage (I-V) characteristics reminiscent of the Kosteritz-Thouless transition; the Ohmic dependence is maintained down to 0.9 K, below which nonlinear dependence of $I \propto V^{\alpha}$ appears with α increased up to 2.5 at 0.7 K, as shown in

Fig.3-7. This fact leads us to speculate that in-plane gradual transition above 1 K is a manifestation of the thermally exited vortex-antivortex unbinding. However, somewhat sample-dependent results of the *I-V* characteristics, which may come from difficulty in reliable in-plane electrical measurements of such an extremely anisotropic material, require further investigation before the origin of this peculiar behaviors is concluded. In any case, the fact that the resistive and diamagnetic signals appear only within the layer is an indication of the high two dimensionality.

3.5. *parallel-field-penetration depth*

In Section 3.3., it is mentioned that in the out-of-plane geometry $-4\pi\chi'$ was largely reduced from unity due to the large penetration depth. In this geometry of the ac field against the crystal, the field can penetrate both from the plane in the direction perpendicular to the layers and from the edge in the parallel direction. The former (in-plane) depth, which characterizes length scale of the shielding current flowing within the layer, is roughly given by the London penetration depth, which is of order of 1 μm at most, as discussed in the next section. This is much smaller than the thickness of the crystal. Therefore, the latter(out-of-plane) penetration depth, $\lambda_{\perp}$, is responsible for the considerable reduction of $-4\pi\chi'$ from unity. This is a common situation to the weakly coupled layered organic superconductors.[21)30)] The penetration depth is given implicitly by the following relation.

$$-4\pi\chi' = 1-\left(\frac{2\lambda_{\perp}}{L}\right)\tanh\left(\frac{L}{2\lambda_{\perp}}\right)\cdots\cdots\cdots(3-1) \quad ,$$

where L is the sample length shown in the inset of Fig. 3-9. This formula with the value of L and χ' gives the temperature dependence of $\lambda_{\perp}$. Figure 3-8 shows $\lambda_{\perp}(T)$ deduced from the result in Fig. 3-5 and the value of $\lambda_{\perp}$ at the lowest temperature available is found to be 1.65 mm. Reproducibility of this result was examined by the measurements of five crystals with different dimension, L. All of the samples showed the similar temperature dependence of $-4\pi\chi'$ as shown in Fig. 3-5. The values of $-4\pi\chi'$ at 0.4 K for the five

crystals are plotted as a function of crystal length, L, in Fig. 3-9. All of the results are fitted with excellent quality to a solid curve given by Eq. (3-1) with $\lambda_{\perp}$=1.65 mm. The $\lambda_{\perp}$ deduced from Eq. (3-1) for each sample is shown in the inset of Fig. 3-9. These results guarantee reliability of the value of the penetration depth. The measurements was extended down to 50mK using the dilution refrigerator by Nakazawa et.al ,[31] who reported that $\lambda_{\perp}$ at zero temperature limit is 1.4mm. This value is consistent with the values extrapolated to 0 K in the present $\lambda_{\perp}$. Thus it is concluded that the $\lambda_{\perp}(0)$ of α-ET is 1.4mm. This value is considerably large, of which origin and comparison with other superconductors will be discussed in Section 3.7.

3.6 *Anisotropy parameter ; anisotropy of resistivity and penetration depth*

Another important parameter is the in-plane penetration depth, $\lambda_{//}$, which could not be determined in the present experiments. Then the $\lambda_{//}$ is estimated by Eq. (1-8) and a value of 0.17 μm is obtained, using a hole density of $n = 9.96 \times 10^{20}$ [cm^{-3}] and assuming the free electron mass. If a value of electron mass in α-ET is the same as one calculated from the penetration depth measured in κ-ET, $\lambda_{//}$ in α-ET amounts to 0.9 μm, where $\lambda_{//}$ in κ-ET was measured by several workers[32)33)34)] with several methods and almost converge. It should be noted that the electron mass of κ-phase superconductors is enhanced by the electron-electron correlation. So the obtained value of $\lambda_{//} = 0.9$ μm can be considered to be an upper limit. This result gives anisotropy parameter $\gamma = \lambda_{//} / \lambda_{\perp} = (m_{\perp} / m_{//})^{1/2}$ in a range of 1500~8000. As discussed in Section 3.1, the anisotropy of resistivity is in a range of ~ 10^6, which is roughly consistent with the above calculation because of the relation of $\lambda_{//} / \lambda_{\perp} = (\sigma_{\perp} / \sigma_{//})^{1/2}$. This value of γ is one order of magnitude lager than those of BSCCO (γ=150) and κ-ET (γ=250), which is known to be highly two-dimensional.

3.7. *Discussion*

As expected from crystal structure in Section 1.5, the quasi-two-dimensional nature of superconductivity was observed in α-ET in both the resistive and inductive measurements. Such a anisotropic behavior has never been observed in any superconductor to date to our knowledge. Moreover, the in-plane character is suggestive of the Kosteritz-Thouless (K-T) transition. While the K-T transition is believed to occur in the superconducting thin film beyond dispute, there is controversy about the occurrence in the bulk layered system. In the early stage of the study of the single crystal of BSCCO, several reports suggested the K-T transition.[35)36)37)] Since then the controversial results were also reported and the conclusion does not converge. As is seen below, the two-dimensionality of superconductivity is more enhanced in α-ET than BSCCO. This situation seems favor of the possibility of K-T transition in α-ET. Although the mechanism of the behavior cannot be specified yet at present, it should be associated with the highly two-dimensional character, which is the most peculiar feature of α-ET.

The out-of-plane ac susceptibility gave the out-of-plane penetration depth, $\lambda_\perp(0)$, as a macroscopic value of 1.4mm. For comparison, the values of $\lambda_\perp(0)$ for several organic superconductors are listed in Table 3-1.

Table 3-1. The out-of-plane penetration depth for several organic superconductors.[21) 30)]

organic superconductor	$\lambda_\perp(0)$ (μm)
κ-(BEDT-TTF)$_2$Cu(NCS)$_2$	200
κ-(BEDT-TTF)$_2$Cu[N(CN)$_2$]Br	200
κ-(BEDT-TTF)$_2$Ag(CN)$_2$H$_2$O	80
κ-(MDT-TTF)$_2$AuI$_2$	<20

It is found that the value of α-ET is one or two orders of magnitude larger than those of other organic superconductors. Since $\lambda_\perp$ proves the interlayer superconducting coupling, this results shows extremely week coupling between the superconducting layer. In a model of Joshphson-coupled multilayer, with using Eq.1-5 and Eq.1-6, the out-of-plane penetration depth at 0 K is given by

$$\lambda_\perp = \left[\frac{4\pi^2\Delta}{\hbar c^2 \rho_\perp}\right]^{-\frac{1}{2}}$$

with Δ, the gap parameter. Assuming the weak coupling BCS relationship, $\Delta=1.76k_BT_c$, with T_c =0.95 K in the present case, the value of $\rho_\perp$=20-40Ωcm gives $\lambda_\perp$=0.5-0.7mm. This value is somewhat smaller but of the same order of magnitude as the experimental value. In the Josephson-coupled model, the two-dimensional character of the individual layer is assumed to be bulklike with the BCS weak coupling nature. The difference between the experimental and calculated values may come from two-dimensional order-parameter fluctuations inherent in the individual layer in the real layered system.

The anisotropy of the penetration depth and resistivity of α-ET was listed in Table.3-2 with those of BSCCO and κ-(BEDT-TTF)$_2$Cu(NCS)$_2$ (κ-ET).

Table 3-2. Anisotropy parameters of α-ET, κ-ET[20) 38)] and BSCCO.[20) 26)]

	α-ET	κ-ET	BSCCO
$\lambda_\perp/\lambda_{//}$	1500~8000	~250	~150
$\rho_\perp/\rho_{//}$	~10^6	~10^3	~10^5

In the three quasi-two-dimensional superconductors, the relation of $\lambda_{\perp} / \lambda_{//} = (\rho_{\perp} / \rho_{//})^{1/2}$ seems to hold fairly well. The two kinds of anisotropy parameters are found to be both larger in α-ET than in other two superconductors, which are known as quasi-two-dimensional ones with the highest anisotropy among each family. The present compound may have the highest anisotropy among all the bulk-superconductors to date.

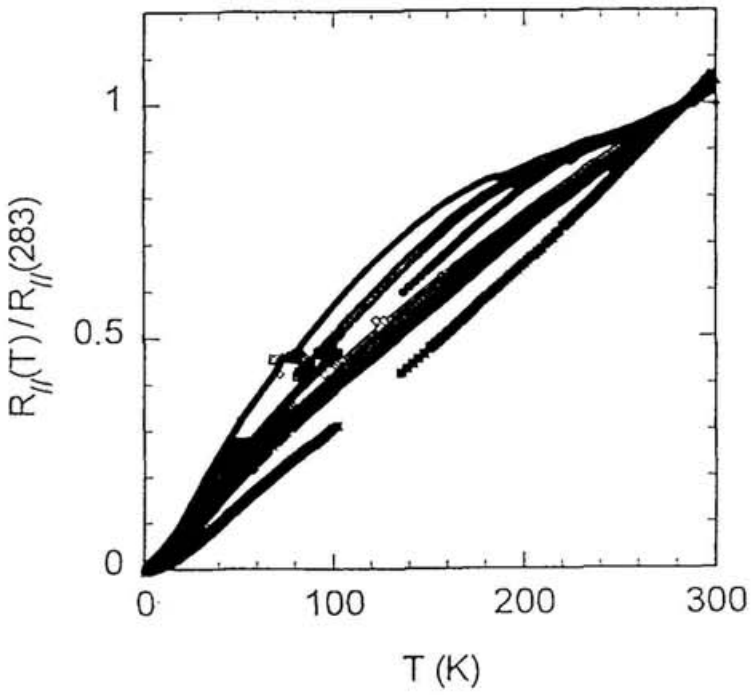

Fig. 3-1. In-plane resistance normalized at 283K for 8 crystals.

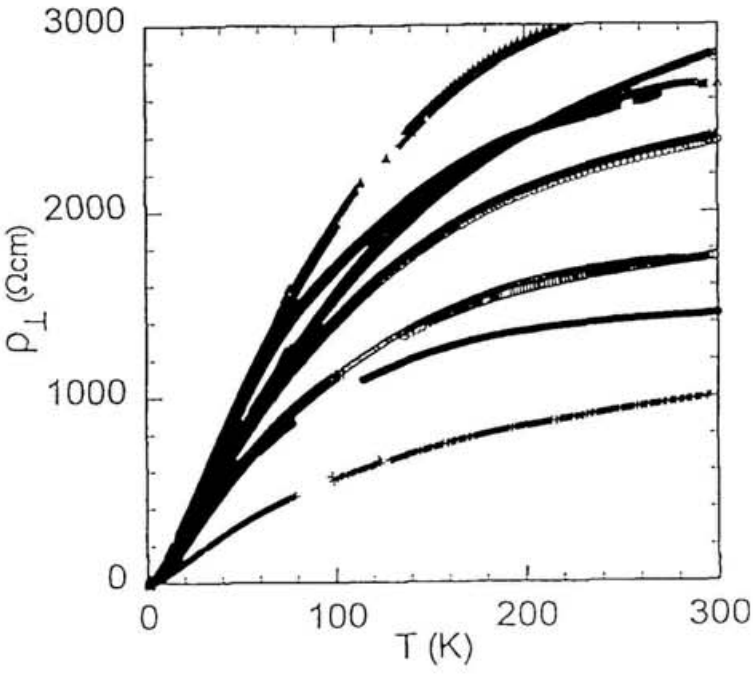

Fig. 3-2. Out-of-plane resistivity for 11 crystals.

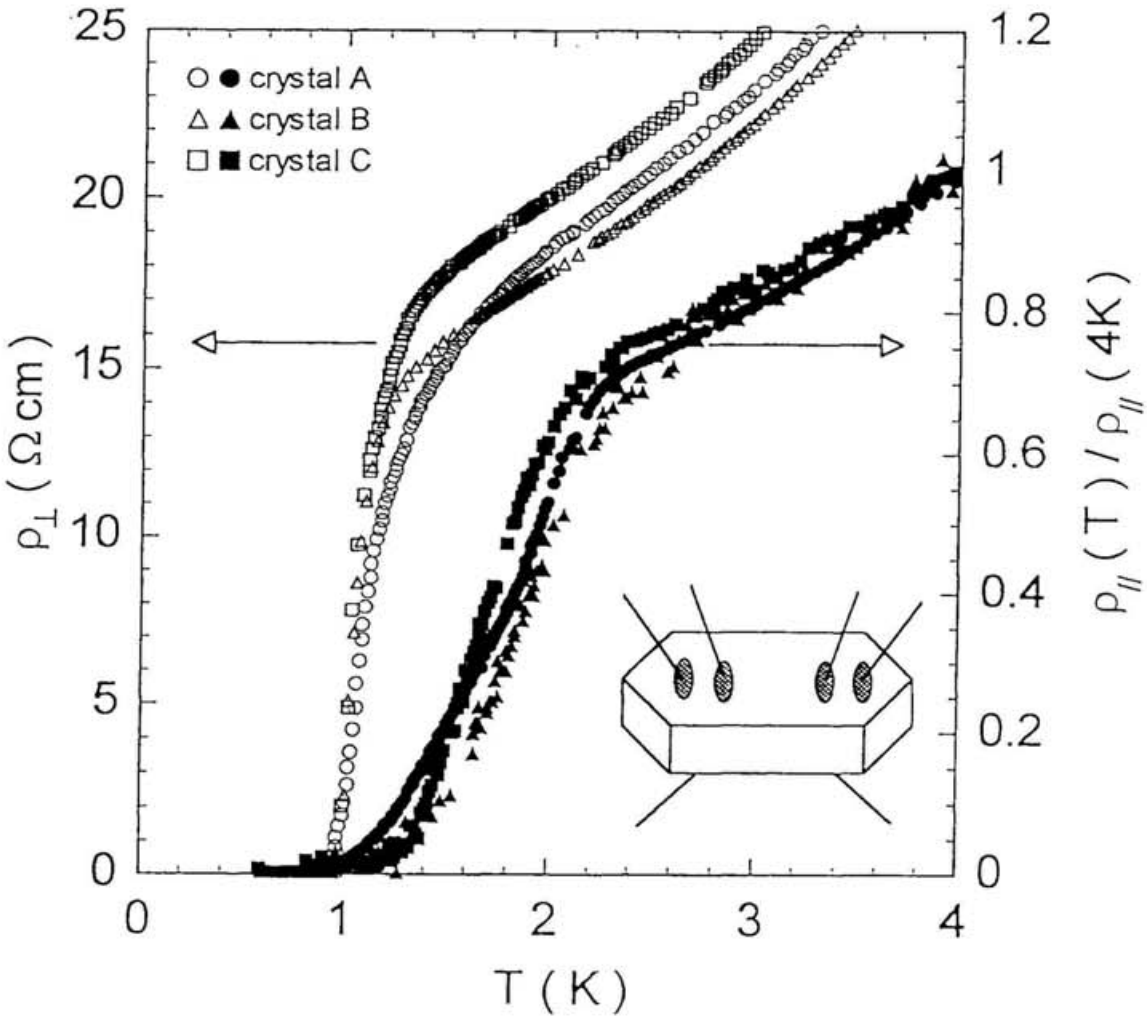

Fig.3-3 In-plane ($\rho_{//}$) and out-of-plane ($\rho_{\perp}$) resistivities measured with sixterminal method for three crystals. $\rho_{\perp}$ is absolute values while $\rho_{//}$ is normalized to the value at 4 K.

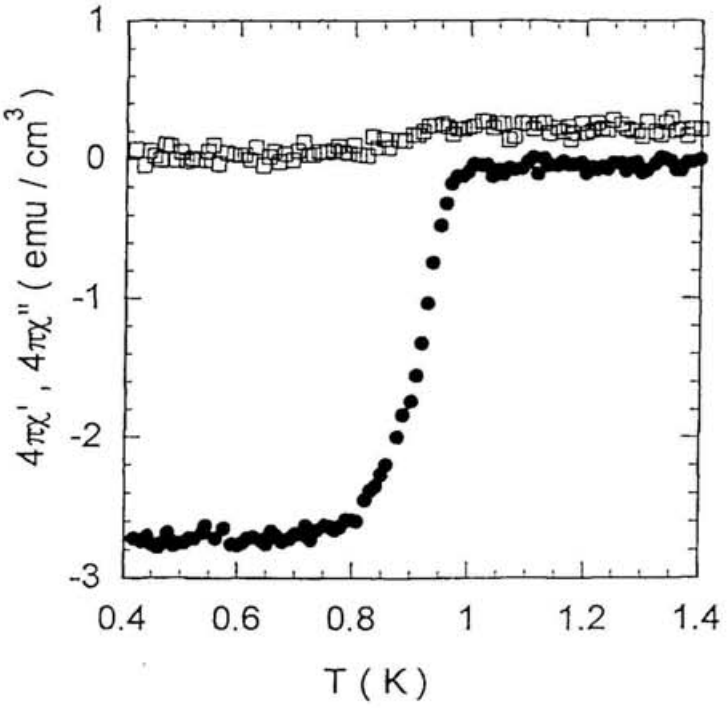

Fig. 3-4. ac susceptibility measured under an ac field of 47 Hz and 0.16 Oe (in amplitude) perpendicular to the layer.

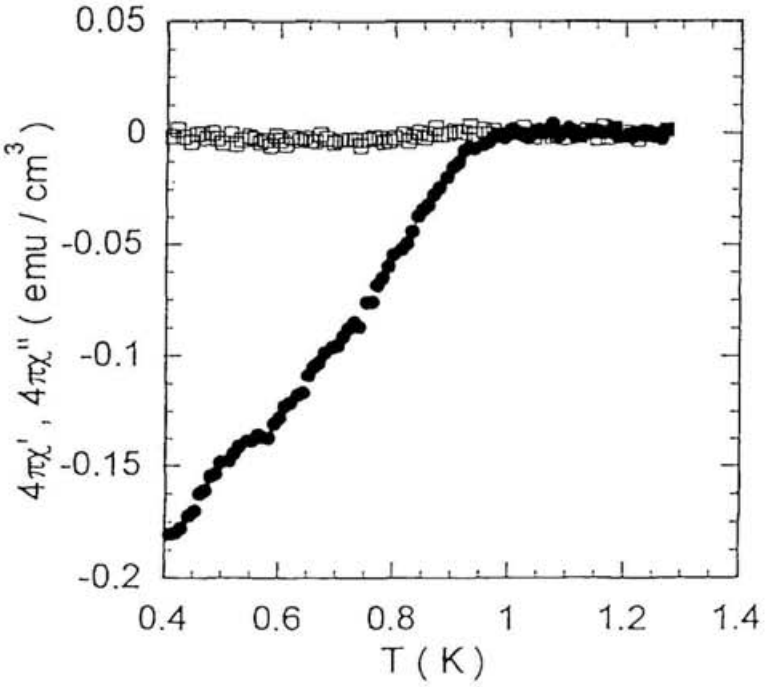

Fig.3-5. ac susceptibility measured under an ac field of 1007 Hz and 0.16 Oe parallel to the layer.

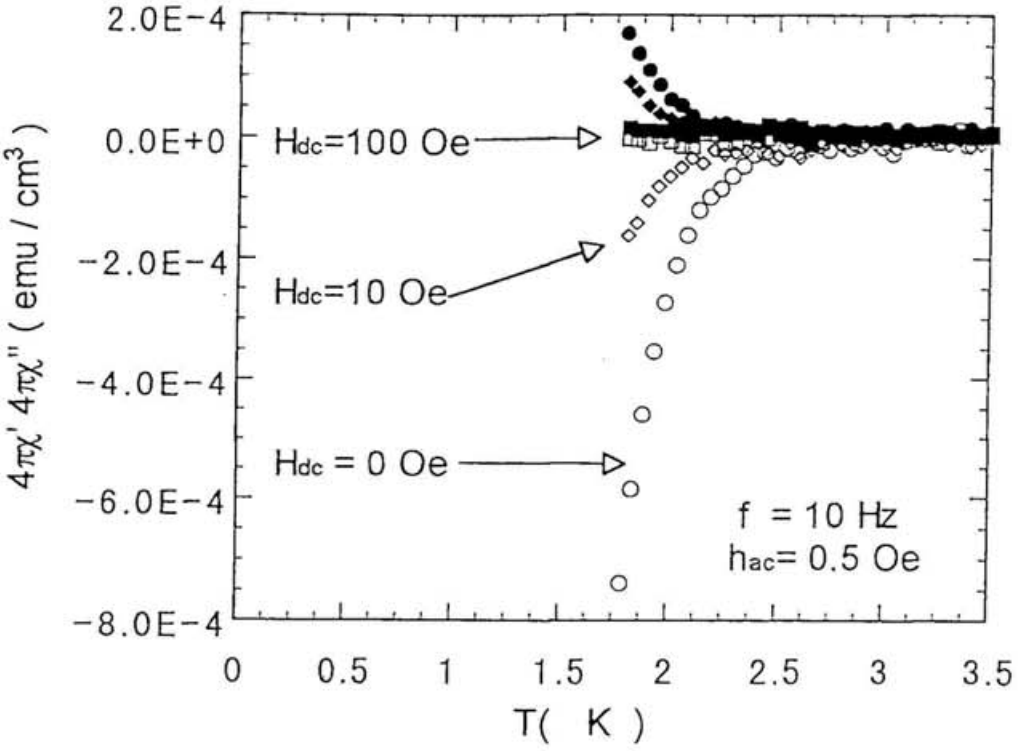

Fig.3-6. High resolution in-plane ac susceptibility measured in SQUID magnetometer

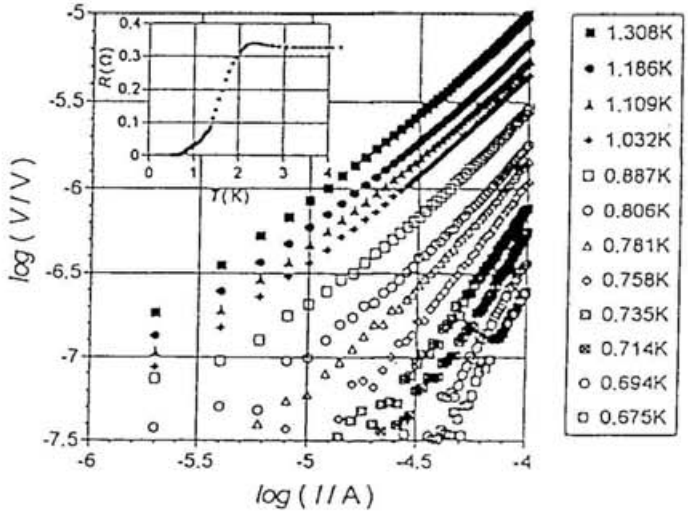

Fig. 3-7 *I-V* characteristics in in-plane configuration

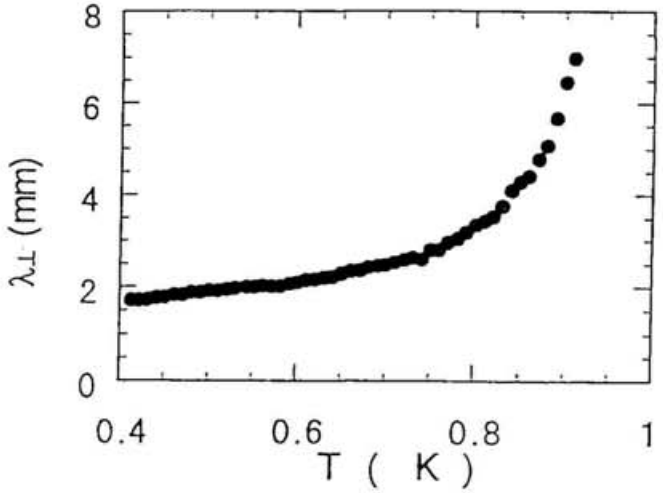

Fig. 3-8. Parallel field penetration depth deduced from susceptibility data (Fig. 3-4)

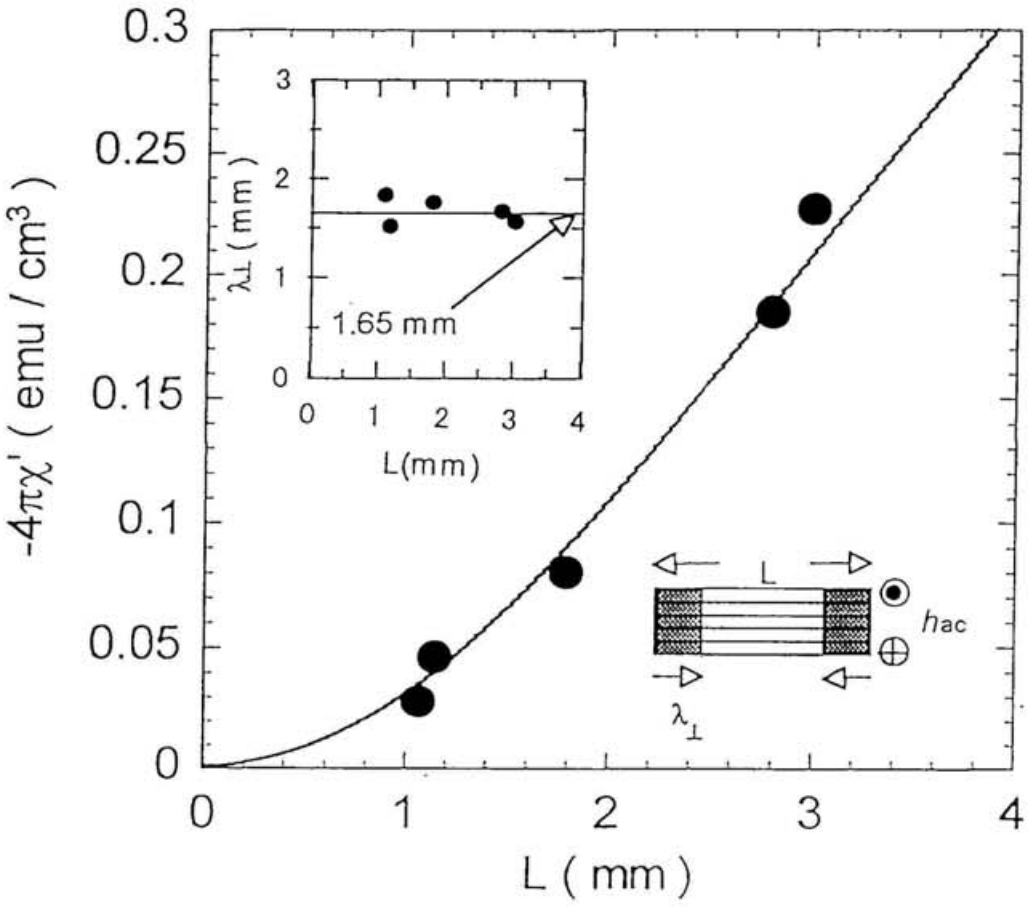

Fig. 3-9. The out-of-plane ac susceptibility vs sample size for five crystals. Inset shows the values of $\lambda_\perp$ deduced through Eq.(3-1) for each crystal. The values are well fitted by a value of $\lambda_\perp$=1.65 (mm), as shown by the solid curve and line.

4. *Characteristics of vortex state under perpendicular magnetic field*

4.1. *Specific heat ; characterization of mean-field upper critical fields*

In the previous chapter, penetration depths, $\lambda_{//}$ and $\lambda_{\perp}$, and the anisotropy parameter, γ, were discussed. In the superconductive parameters, coherence length, ξ, which can be determined from H_{c2} line in Ginzburg-Landau theory, is quiet important. In a superconductor, which have large fluctuations of vortices, resistivity is not an useful probe for definition of $H_{c2}(T)$, because the superconducting fluctuations in a higher temperature side and the fluctuations of vortices (flux flow) in lower temperature side make the resistive $H_{c2}(T)$ line ambiguous. It is also believed that physical quantities in such a system does not show so clear transition at $H_{c2}(T)$ under fields as in the conventional superconductors. One of the reasonable definitions of the mean-field-like $H_{c2}(T)$ is by the thermodynamic quantity. Figure 4-1 shows electronic specific heat of this material obtained by Nakazawa[39] in our laboratory. The data of C_p / T in several magnetic fields are plotted, where C_p is difference between specific heats in the normal and superconducting states, i.e., $C_p = C(H) - C(H = 8\mathrm{T})$. It is noted that the system is in the normal state in a field of 8T. Assuming the mean-field transition curves predicted by BCS theory as shown by the solid line, the transition temperatures, $T_c(H)$, were determined in each field so that they compensate the entropy from the thermodynamic point of view. Thus, a $H_{c2}(T)$ line was defined by a set of the $T_c(H)$ data as a characteristic boundary of occurrence of superconductivity. Figure 4-2 shows the results of the present two crystals and the previous results reported by Andraka et al.[40] Temperature derivative of upper critical field near T_c was obtained as $-(\mathrm{d}H_{c2}(T)/\mathrm{d}T)_{Tc} = 0.08$ T/K from the

present data; this value is slightly different from $-(\mathrm{d}H_{c2}(T)/\mathrm{d}T)_{Tc} = 0.1 \pm 0.02$ T/K determined by Andraka et al.[40] who defined T_c (H) as the temperature giving the maximum in C / T. Using the present value and the Ginzburg-Landau theory, the G-L coherence length, ξ_{GL} , is estimated at about 500 Å.

4.2 *Superconducting parameters; extremely enhanced anisotropy and large fluctuations of vortices*

In this section, characteristics of the superconducting parameters of α-ET (α-(BEDT-TTF)$_2$NH$_4$Hg(SCN)$_4$) are discussed. The superconducting parameters obtained from the experimental and the inference in the previous sections are all listed in Table 4-1 with those of two quasi-two-dimensional superconductors, κ-ET (κ-(BEDT-TTF)2Cu(NCS)$_2$) and BSCCO ($Bi_2Sr_2CaCu_2O_{8+\delta}$).

Table 4-1. Superconducting parameters of α-ET, κ-ET[20] and BSCCO.[20]

Parameter	α-ET	κ-ET	BSCCO
T_c (K)	0.95	9.5	91
$\xi_{//}$ (Å)	500	60	30
$\lambda_{//}$ (μm)	0.17～0.9	0.8	0.26
$\lambda_{\perp}$ (μm)	1400	200	40
γ	1500～8000	250	150
s (Å)	20	15	15
γs (μm)	3～16	0.4	0.2

As discussed in Chapter 1, these parameters dominate the character of the vortex state, so that the knowledge of them is quite informative to argue the *H-T* phase diagram with the experimental results. The Ginzburg number, *Gi*, of α-ET can be calculated by Eq.(1-3) with the above parameters. The obtained value is about 0.1, which is

considerably larger than that of Nb (5×10^{-7}) and also larger than that of $YBa_2Cu_3O_{7-\delta}$ (0.01). Because *Gi* measures the size of fluctuations of the vortices, a larger value is expected to give a wider range of the vortex liquid phase in *H-T* plane, as was discussed in Chapter 1.

Another feature of the parameters of α-ET, distinctive from other materials, is the large in-plane Ginzburg-Landau coherence length, $\xi_{//}$, which is one order of magnitude lager than those of other two superconductors. This is partly because of the low transition temperature.

As for the parameters related to anisotropy or strength of the out-of-plane coupling, the anisotropy parameter, γ, and concomitantly the out-of-plane penetration depth, $\lambda_{\perp}$, are even lager than those of κ-ET and BSCCO, which belong to a class of highly anisotropic superconductors. One of the reasons giving extremely high γ is the layer spacing (s = 20 Å) larger than those of the others (s = 15 Å).

These features give a distinctive aspect of α-ET; Josephson length, γs, is larger than in-plane penetration depth, $\lambda_{//}$. The relation of $\gamma s > \lambda_{//}$ indicates that this superconductor is classified as an extremely-anisotropic-class superconductor, while $\gamma s < \lambda_{//}$ in BSCCO and κ-ET. [The $\lambda_{//}$, of course, depends on temperature and diverges near T_c. However, the difference by one order of magnitude between γs and $\lambda_{//}$ means that the relation of $\gamma s > \lambda_{//}$ holds in a wide temperature range except the vicinity of T_c in α-ET.] In a quasi-two-dimensional system, the tilt modulus of the vortices, C_{44}, is determined by the Josephson contribution and the electromagnetic one, of which the typical line energy scales are $(\Phi/\gamma s)^2$ and $(\Phi/\lambda_{//})^2$, respectively. In this sense, the pancake vortices in α-ET are mainly coupled through the electromagnetic energy especially in low

temperature region, while those in κ-ET and BSCCO are dominated by the Josephson energy. This feature distinguishes the present system from the other systems and, therefore, may affect the vortex state, giving a possible variation in the H-T phase diagram.

4.3 *ac susceptibility in the vortex state*

The ac susceptibility under fields reflect the mobility of vortices. Therefore, a change of signal in the vortex state in this measurement is an indication of a change of their mobility. The experiments were performed in both in-plane and out-of-plane configurations of ac fields, which were explained in Section 3.3. The dc fields were applied in a direction perpendicular to the conducting layers all through the present work. In the in-plane configuration, the ac field perpendicular to the plane causes the vortex motion in the compression mode, while in the other configuration the ac field parallel to the plane acts on the tilt mode. The measurements in these two configurations lead us to understand the mobility of vortices in the two modes.

The in-plane ac susceptibility was measured with an ac field of 0.17 Oe in amplitude under zero and several dc fields. From the ac-amplitude dependence of susceptibility, 0.17 Oe is confirmed to be in the low-amplitude limit. The frequency of ac field is 17 , 47 , 307 and 1007 Hz. Figure 4-3 shows in-plane susceptibility at 1007 Hz. The transition curve shifts to lower temperature side in higher dc field without losing its sharpness. The χ' and χ'' show an appreciable frequency dependence; the transitions shift to lower temperatures at lower frequencies, which will be discussed in Section 4.5.

The out-of-plane ac susceptibility is shown in Fig. 4-4. An applied ac field is 0.17 Oe in amplitude and 1007 Hz in frequency. The transition curves in χ' do not saturate and the absolute value reaches only 15 % of the full Meissner value even at 0.5K. The reason of this behavior was discussed in Section 3.3. The transition curves shift to the lower temperature side in higher dc fields as in the in-plane configuration. The out-

of-plane susceptibility does not show frequency dependence in a measured range of 107-3007 Hz.

4.4. *Resistivity in the vortex state*

The resistivity measurements were performed in both the in-plane and out-of-plane configurations under perpendicular dc fields, where the dc current was injected in directions parallel and perpendicular to the conducting layers, respectively. Figures 4-5 and 4-6 show the in-plane and out-of-plane resistivities under several dc fields, respectively. In this superconductor, the normal-state in-plane resistivity just above T_c is quite small compared with other BEDT-TTF salts. Reflecting a small H_{c2} value, a comparatively low field range should be studied. Because the flux flow resistivity is proportional to the normal state resistivity and an applied field in the Bardeen-Stephen context for example, the measurement of in-plane resistivity in the vortex state in question requires quite high resolution and therefore it is not straightforward to deduce information about the mobile vortices from the in-plane resistivity. This is also because the injection current must be too small to cause heating in such a low-T_c superconductor. However, the out-of-plane resistivity, $\rho_{\perp}$, which is several orders of magnitude larger than in-plane resistivity in the normal state, is observable with moderate sensitivity. In a superconducting state, the out-of-plane resistivity probes the coherence between the layers, so that it is accessible to make an experimental study on the out-of-plane correlation in the vortices.

In the out-of-plane configuration, the injection dc current was 10 μA, where the linearity of the *I-V* characteristic was maintained in this low current range over the whole temperature and field region. When dc fields are increased, the transition curves shift to the lower temperature side, as seen in Fig. 4-6. And, interestingly, its sharpness is scarcely

lost by application of dc fields. This behavior does not seem to be shared by other quasi-two-dimensional superconductors. In BSCCO, the more field is applied, the broader the transition is.[4)] It is reported that the resistivity follows an activation-type in both directions and that the activation energy is almost same in the two directions.[41)] In this literature, the behavior was considered to indicate the dynamics of unconnected pancakes, which will explain the independence of activation energy on the current direction. In this sense, the out-of-plane resistive curves of α-ET is considered to come from a different mechanism. Through the above discussion, it is suggested that the decrease of the out-of-plane resistivity reflects a rapid increase of the out-of-plane coherence rather than a decrease of the in-plane mobility of the pancake vortices.

4.5. *Simultaneous change of vortex mobility in the two modes; onset of inductive transition*

The onset of the inductive transition in the vortex state in in-plane and out-of-plane χ' marks a drastic change of the vortex mobility. In the in-plane ac susceptibility, the onset temperature does not depend on frequency under a zero field but shows an appreciable frequency dependence under fields, as is shown in Figs. 4-7 (H_{dc}=0) and 4-8(H_{dc}=55Oe). This fact suggests that the frequency dependence is attributed to the dynamical response of vortices, not to the effect of the normal skin depth because the in-plane resistive transition shows similar profiles of the gradual transition in a zero and nonzero fields, which would give essentially the same skin effect if it were concerned. On the other hand, the out-of-plane susceptibility shows no frequency dependence under a zero or finite fields within the experimental resolution, as shown in Figs. 4-9(H_{dc}=0), 4-10(H_{dc}=9) and 4-11(H_{dc}=36). The onsets of in-plane and out-of-plane χ' are plotted in the H-T plane in Fig.4-12 along with the Hc_2 line determined by the specific heat measurement, mentioned in Section 4-1.

The qualitative difference of the frequency dependence between the two configurations is considered to come from the different manners to stimulate the motion of the vortices. In the in-plane configuration, the ac field initiates activation of the compression mode of the vortex motion from the crystal peripherals. In this situation, the modulation of the vortex density is transmitted toward the center of the sample through the diffusion process in the mobile-vortex state. Thus the characteristic frequency of the response of the whole vortex system to the ac field in this configuration is determined by

the ratio of the sample size and the diffusion constant, which might give an applied-frequency dependence of the susceptibility profile as crossover behavior.

On the other hand, the ac field in the out-of-plane configuration reaches the whole sample volume due to the peculiarity of this material; the out-of-plane penetration depth is comparable to or larger than the sample size. This feature permits the whole vortices to be driven directly by the out-of-plane ac field, not via the diffusion process. In this case, the characteristic frequency of the system response is that of the dynamics of the individual vortices. The observation of absence of frequency dependence of the out-of-plane χ' in a range of 150-3000 Hz indicates that the dynamics of individual vortex is much slower than this frequency range below the χ' onset temperature and is much faster than that above the onset without a gradual crossover of the characteristic frequency of the vortex dynamics. Thus, the frequency dependence appearing only in the in-plane configuration is attributed to the crossover of *the diffusion process* of the mobile vortices. As seen in Fig. 4-12, the coincidence of the frequency-independent out-of-plane onsets and the in-plane onsets in the low frequency limit corroborates this interpretation.

Therefore, the drastic change of the vortex mobility is likely the phase transition rather than the crossover, and is suggested to be a melting of vortices.

4.6 *Rapid growth of out-of-plane correlation; offset of out-of-plane resistive transition*

Since the out-of-plane resistivity probes the out-of-plane correlation of the pancake vortices, vanishing of the resistivity signs establishment of the out-of-plane coherence. Although the out-of-plane resistive transition is sharp, there are some argument and ambiguity on the determination of the offset of the transition. This is because that the resistive profiles have small tails in low resistive and temperature side.

As seen in the lower panel of the inset of Fig. 4-13, the out-of-plane resistivity approaches zero with a linear temperature-dependence, of which the extraporation to a zero resistivity gives a characteristic temperature of appearance of the out-of-plane phase coherence. Totally five crystals were examined. The results of thus determined temperatures at several fields for each crystal are plotted by different symbols in the field-temperature phase diagram in Fig. 4-14. (The closed circles of smaller sizes represent the different definitions of the offset temperature discussed below.) The results seem to be all on a single curve without serious sample-dependence, supporting that this line is a out-of-plane decoupling boundary of pancake vortices. There may be a case that the tail appearing just before the resistivity vanishes is an intrinsic behavior reflecting the growth of the out-of-plane phase coherence. For the tail part of the resistive transition, however, nonnegligible sample-dependence was encountered and implies that the observation should not be taken as it is. The resistive profiles shown in Fig. 4-13 are those of a crystal with the smallest resistive tail, which is visible in the logarithmic plot in the upper panel of the inset. Considering the tail part, one can make other definitions of

the offset temperatures; for example, the temperatures giving $\rho_n/100$ or $\rho_n/1000$, as shown in the inset, where ρ_n is the normal state resistivity at 2K. Thus defined temperatures are plotted by closed circles of the middle and small sizes, respectively, in Fig. 4-14, where the characteristic temperatures are slightly shifted to the lower temperature side. Such a kind of freedom of the definition may make the experimental determination of the decoupling line ambiguous and one may pursue the temperature where the resistivity really vanishes. In case of the in-plane resistivity measurements to probe the vortex melting transition, the search of the vanishing point by the ultra-high resolution measurements is meaningful and the transition point should be determined in this way because the vortex flow resistivity is completely lost by solidification of the vortices. However, it should be noted that the out-of-plane resistivity comes from a different mechanism, namely out-of-plane phase fluctuations. In this mechanism, it is reasonable to consider that the out-of-plane resistivity does not perfectly vanish even when the out-of-plane correlation of the pancake vortices are established, because tilting vibrations contribute to the finite resistivity in the out-of-plane direction. Thus, we consider that the temperature characterized by the linear extraporation corresponds to the decoupling temperature where the phase coherence is practically established/lost, although this is not conclusive. If the decoupling were the first order transition, a jump of the out-of-plane resistivity would have been observed. The absence of such a behavior suggests that the decoupling is a continuous transition (higher than the second order) or a crossover.

4.7 *Discussion*

The onsets of the out-of-plane χ' as the inductive transitions in the low frequency limit and the offsets of the out-of-plane resistivity are again plotted in Fig. 4-15(a)(b) along with the H_{c2} line. This figure includes two additional onset data of the out-of-plane χ' measured in a dilution refrigerator.[31] In this section, these two kinds of boundaries in the vortex state are discussed in terms of the existing theories.

The χ' onsets are fitted by a relation of $H_m=H_0(1-T/T_c)^{\alpha}$, as predicted by the melting theory with fitting parameters of H_0 and α. The thick solid line is a fitting curve and the obtained values of the parameters are 592 G and 2.05, respectively. Also shown in the figure for comparison are two H_m curves with exponrnts of α=1.5 and 2.5, which are seen not to fit the data. The recent melting theory [42] predicts α=2 for the extremely anisotropic case ($\gamma s>\lambda_{//}$) and α=1.5 for the moderately anisotropic case ($\gamma s<\lambda_{//}$) in a low-field region. Since α-ET belongs o the extremely anisotropic case, the fitting value of α is in fairly good agreement with the prediction. It is noted that this theory also explains the experimental value of α of the melting line in BSCCO observed as the first-order transition in the local magnetic measurement (Fig. 1-7). On the other hand, the value of H_0 is given in the theory as follows;

$$H_0 = \frac{\Phi^5 {c_L}^4}{\pi^4 \left(k_B T_c\right)^2 \gamma^2 \lambda_{//}(0)^4} \cdots\cdots\cdots\cdots (4-1) \ .$$

With the experimental value of H_0=592 G and $\lambda_{//}(0)$ of 0.17μm-0.9μm (see Section 3.6),

Eq. 4-1 gives the values of c_L in a range of 0.06-0.14. The value of c_L is considered to be 0.1-0.2 from the experimental and theoretical investigations of high-T_c cuprates. This agreement of c_L strongly support that the boundary in question is a melting line.

Next, the onset of the out-of-plane resistivity, defined by the linear extrapolation argued in Section 4.6, is discussed in the context of the 3D-2D vortex decoupling, which is induced by the competition between the out-of-plane pancake vortex coupling and thermal disturbance. By analogy with Lindemann criterion in melting, the decoupling of pancake vortices is expected to occur when the root-mean-square thermal displacement $u_T=<(u_{n+1}-u_n)^2>^{1/2}$, becomes comparable to the intervortex distance, a_0, where u means the position of pancake vortex in different layers specified by n and $n+1$. Deamen et al.[43] gave a formula of the temperature dependence of the decoupling field, $H_D(T)$, in case of $\gamma s>\lambda_{//}$ (extremely anisotropic case) as follows;

$$H_D(T)=\frac{\Phi^3 s}{32\pi^3 T\lambda_{//}(T)^4}\ln\left(\frac{8\pi^2 T\lambda_{//}(0)^4}{\Phi^2 s^3}\right)\cdots\cdots\cdots\cdots(4-2)$$

If the relation of $\lambda_{//}(T)=\lambda_{//}(0)/(1-T/T_c)^2$ is assumed, a variable parameter in this formula is only $\lambda_{//}(0)$. In Fig 4-15(b), a fit to the data is represented. The best fit gives a value of $\lambda_{//}(0)$=1.47μm. (The curves with $\lambda_{//}(0)$=1.47μm and 1.57μm are also shown for comparison.) As seen in the figure, the functional form of Eq. 4-2 reproduces the experimental data quite well. The fitted value of 1.47μm is not so far from the value of $\lambda_{//}(0)$ evaluated in Section 3.6, but is somewhat larger than that. It is noteworthy that a similar situation was observed in artificial MoGe/Ge multilayers by D.G.Steel et al.[44]

who discussed the decoupling field in the context of Deamen's theory, although it was a case of the moderately anisotropic superconductor. The real decoupling in α-ET occurs at smaller fields than predicted. The case of MoGe/Ge multilayers was reported to be the contrary of one of α-ET. These difference between the observation and the theory may be suggestive of some room for improvement in the theoretical treatment; for example, incorporation of the neglected ingredients such as the effect of the normal core. In any way , it is emphasized that the characteristic line, which is explained qualitatively as the decoupling boundary, was found in the mobile vortex region in the *H-T* plane.

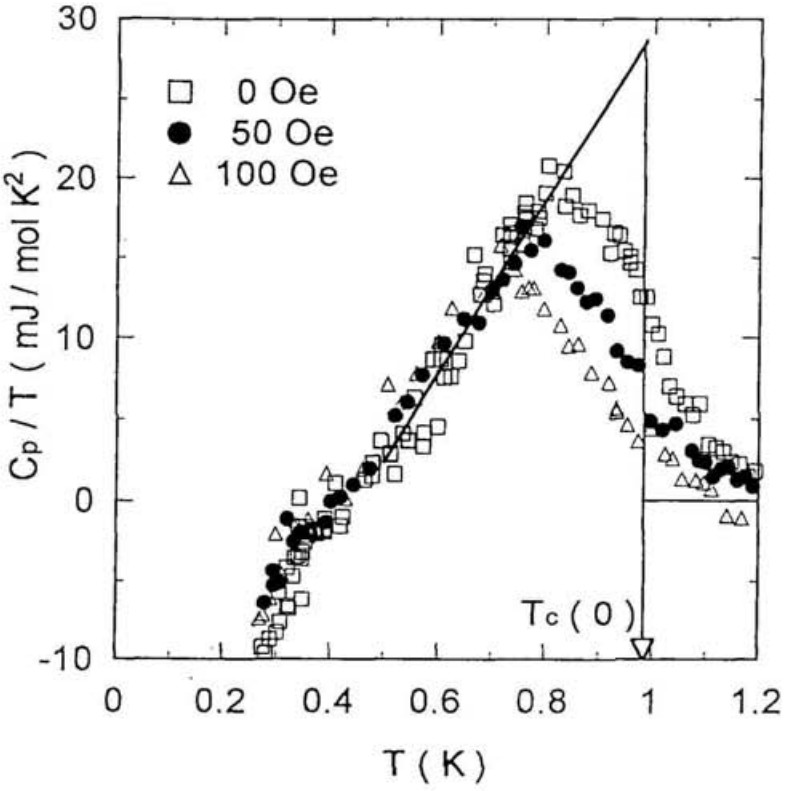

Fig. 4-1. Specific heat difference in between zero and dc fields. $C_p=C(H)-C(H=8T)$

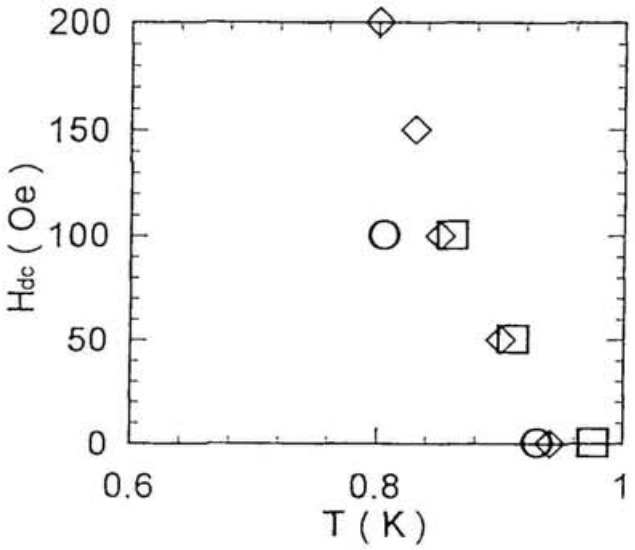

Fig. 4-2. Thermodynamic transition temperatures, $T_c(H)$ for three crystals under fields, which form mean-field H_{c2} line in H-T plane. The symbols, □ and ◇ represent the present data, while the data shown by O are from Ref. 40.

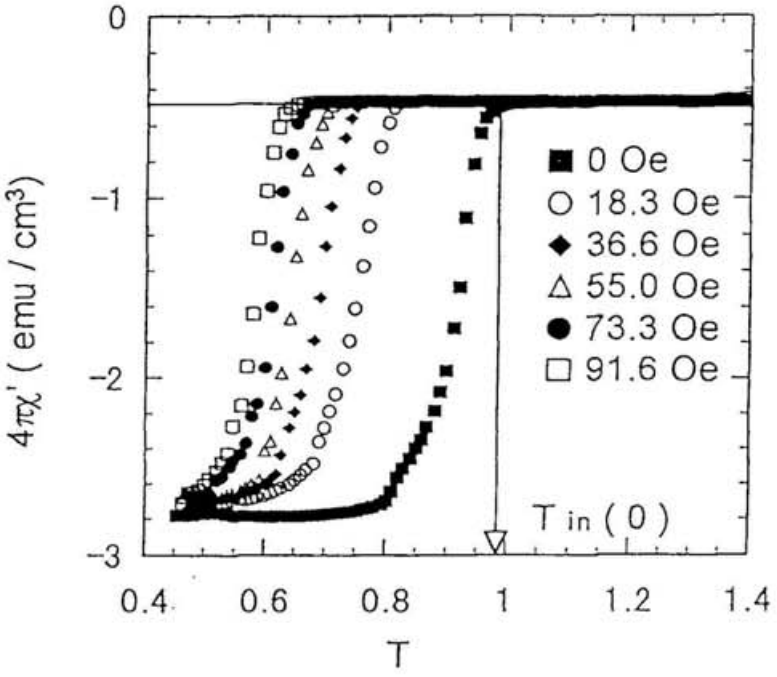

Fig. 4-3 In-plane ac susceptibilities in several dc fields.

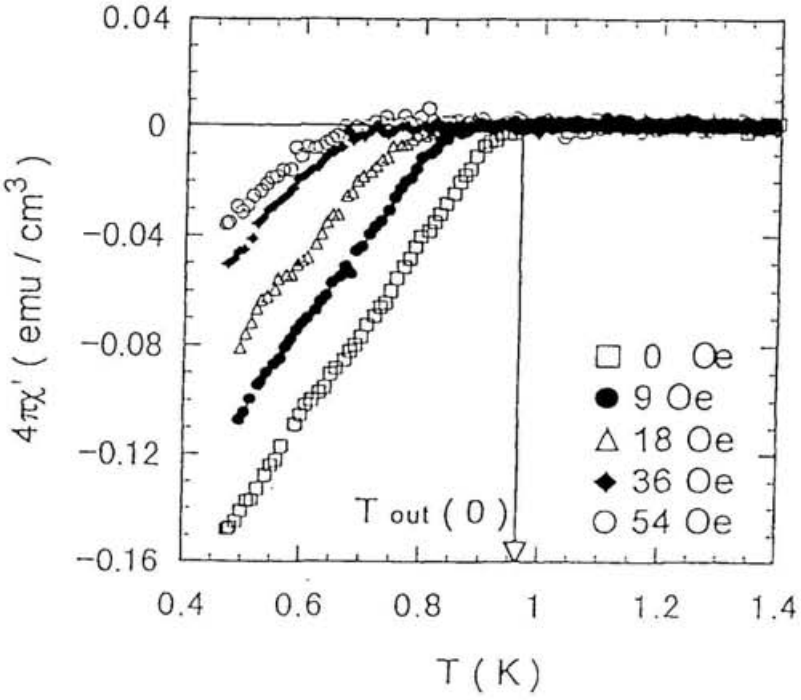

Fig. 4-4 Out-of-plane ac susceptibilities in several dc fields.

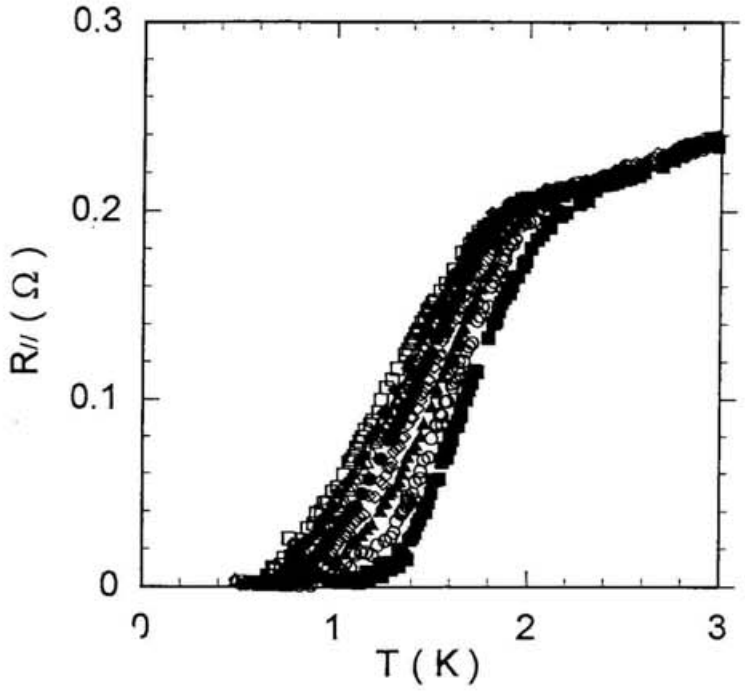

Fig. 4-5 In-plane-resistance, $R_{//}$, in several dc fields. dc fields was applied with a step of 30 Oe from 0 to 210 Oe.

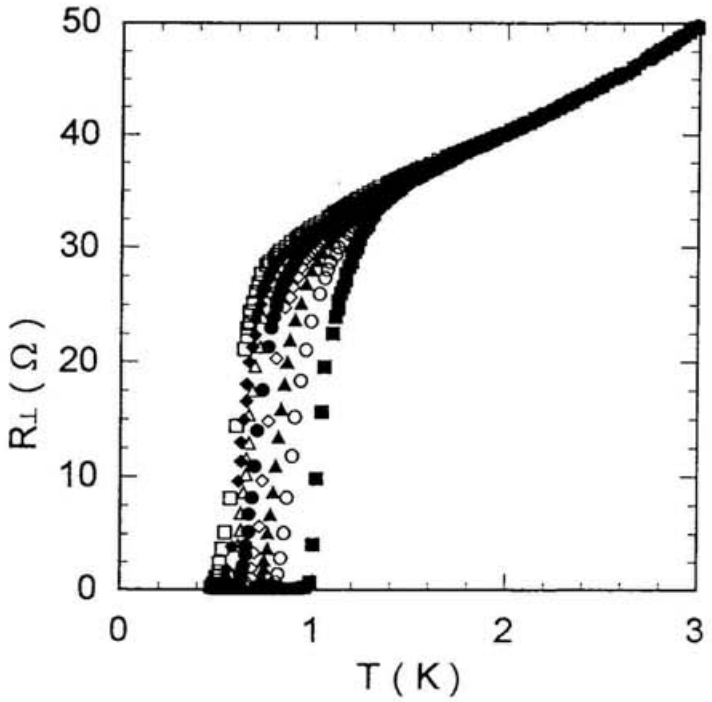

Fig. 4-6 Out-of-plane-resistance, $R_{\perp}$, in several dc fields. dc fields was applied with a step of 30 Oe from 0 to 210 Oe. The above measurement and this measurement were made on the identical sample.

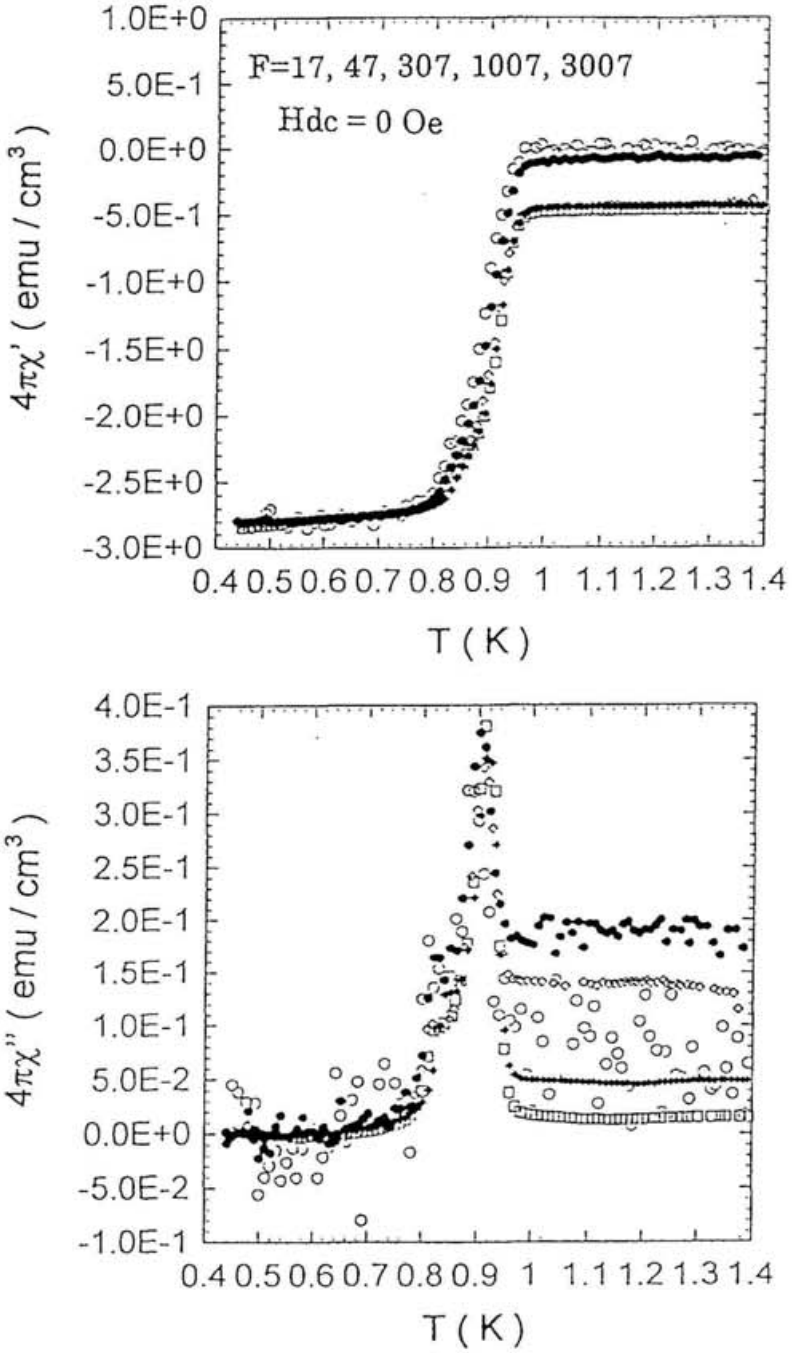

Fig. 4-7 In-plane ac susceptibilities (χ' and χ'') under a zero dc field and ac field of variable frequency. Onset temperature does not show frequency dependence in this measurements.

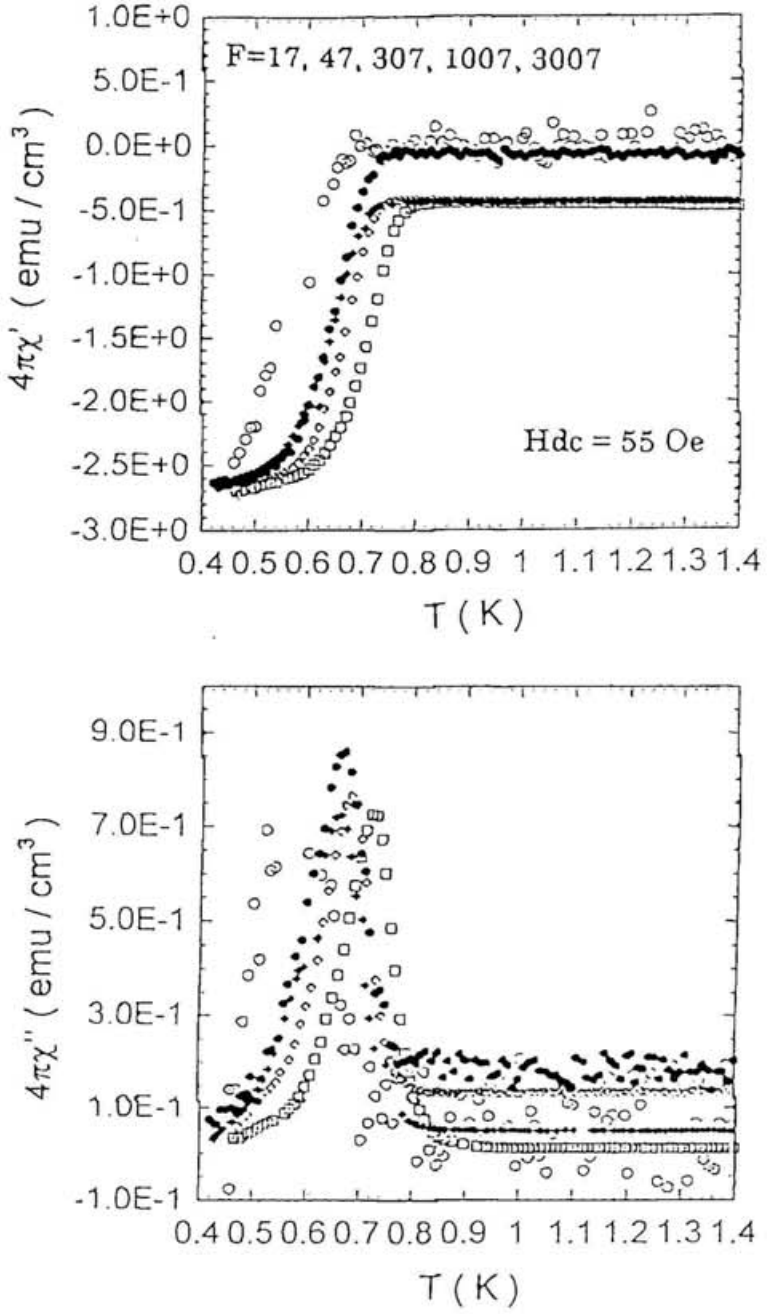

Fig. 4-8 In-plane ac susceptibilities under dc field of 54.96 Oe. A appreciable frequency dependence is shown in both χ' and χ''.

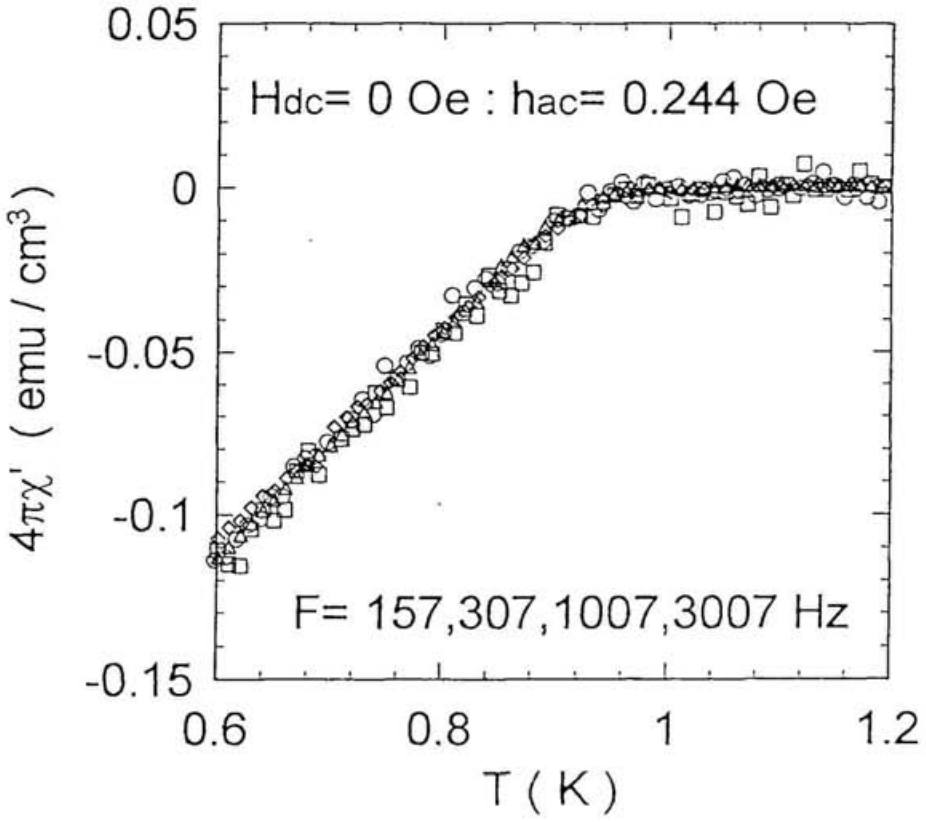

Fig.4-9. Out-of-plane ac susceptibilities under a zero field, which do not show frequency dependence.

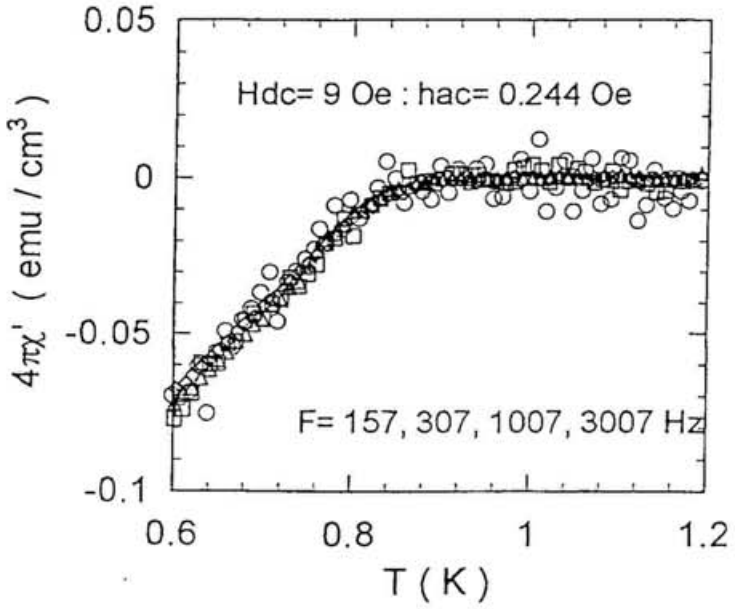

Fig. 4-10 Out-of-plane ac susceptibility under field of 9 Oe. Frequency dependence does not apper.

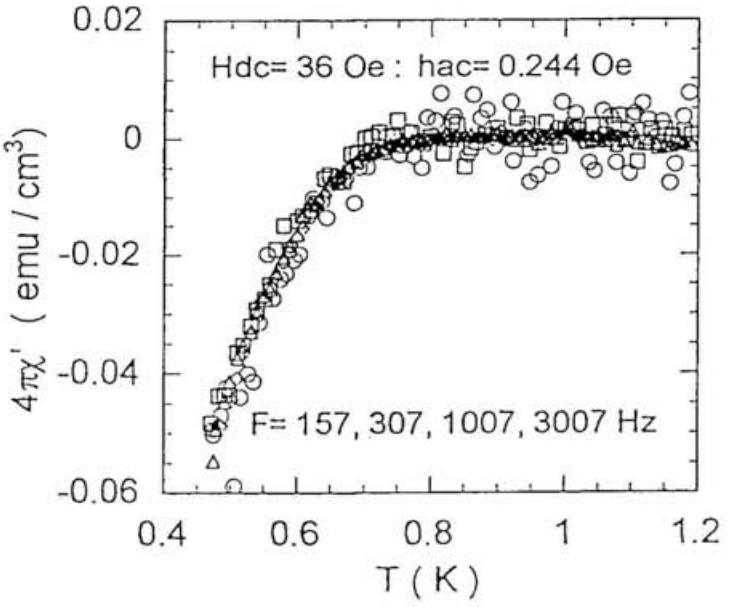

Fig. 4-11 Out-of-plane ac susceptibility under field of 36 Oe.

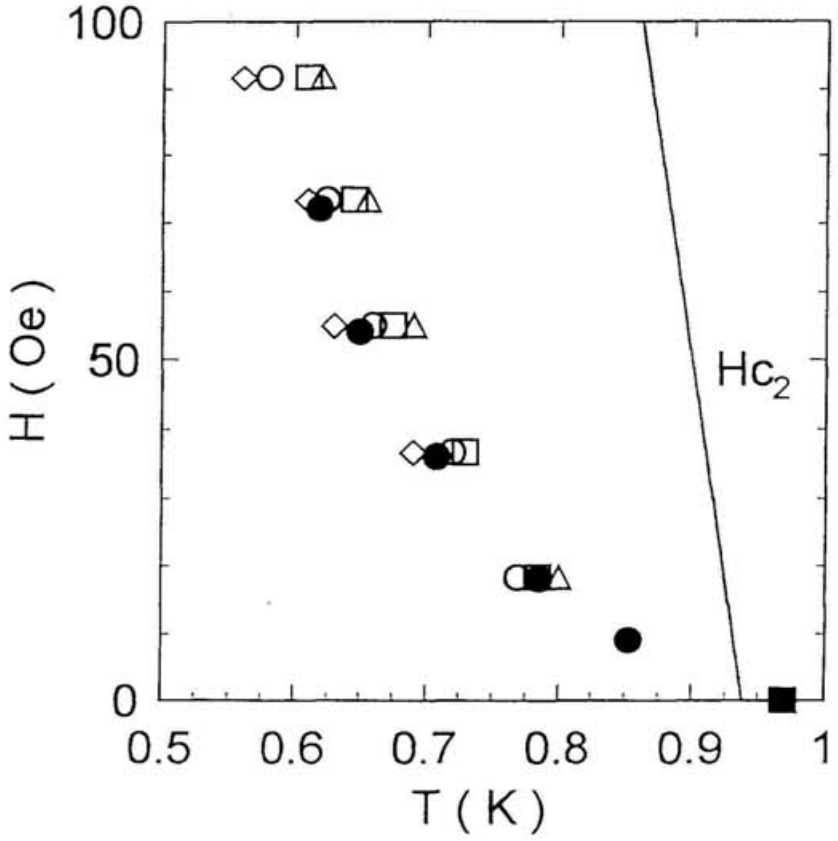

Fig. 4-12. The onset temperatures of the inductive transition. Open symbols stand for frequency dependence of the onsets of in-plame ac susceptibility. Closed circles are the onsets of out-of-plane susceptibility, which does not show frequency dependence.

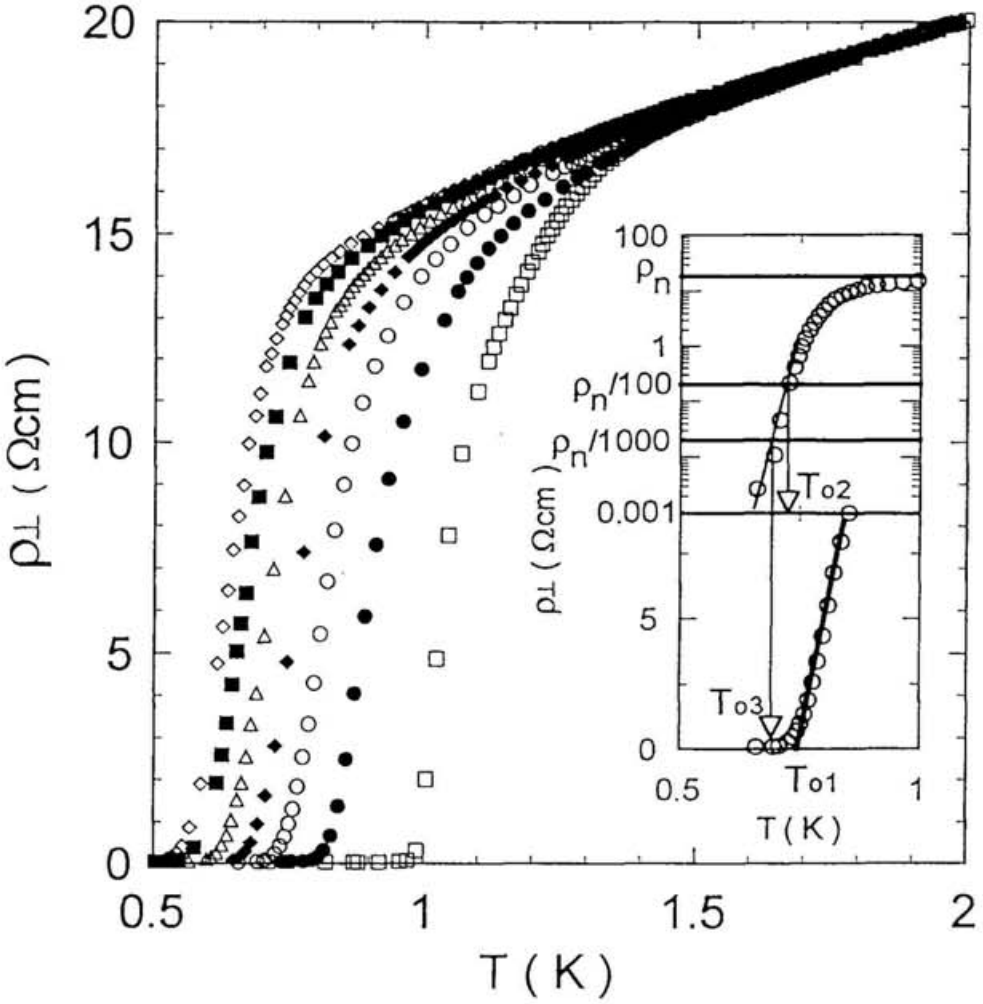

Fig. 4-13. The three criteria of the definitions of the out-of-plane resistive offsets.The out-of-plane resistivity under fields are again shown. Inset:T_{o1} is determined by a liner extrapolation in a lower panel in a liner scale.T_{o2} and T_{o3} are defined by comparison with the rormal state resistance at 2K in upper panel in semi-log scale.

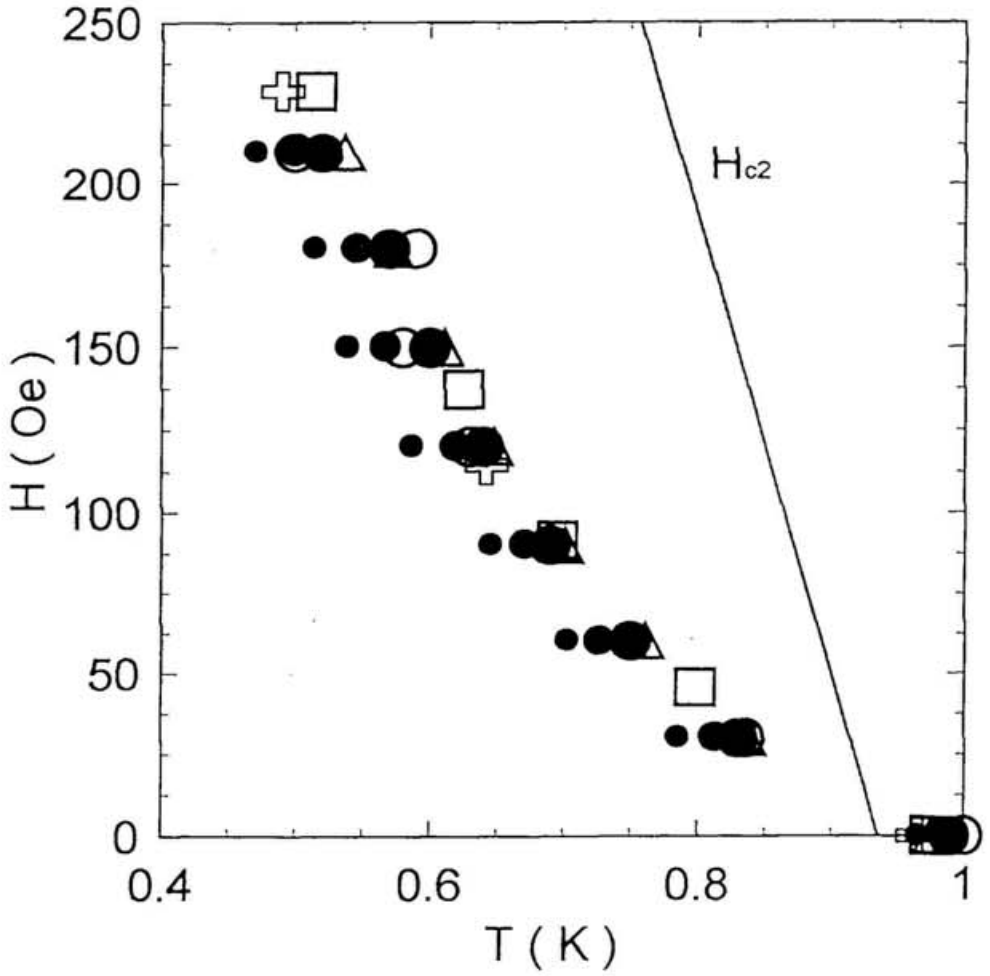

Fig. 4-14. The offset temperatures of $\rho_{\perp}$ for five crystals. Closed circles with different sizes stand for different definition of the offset temperatures for an identical crystal. For definition, see text.

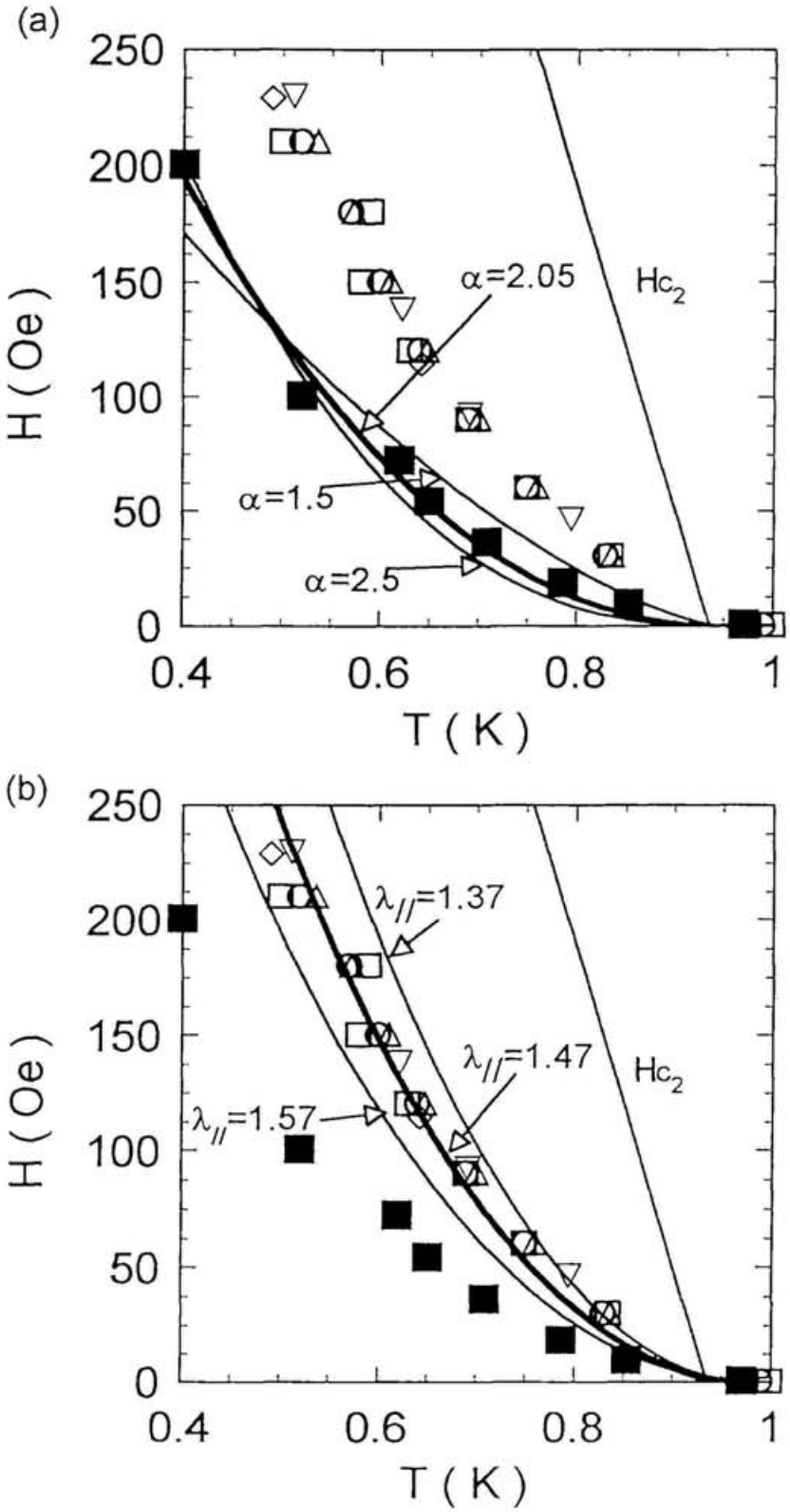

Fig. 4-15. *H-T* phase diagram (a)(b). The onset temperatures of inductive transition and the offset ones of resistive transition are plotted along with the mean-field *Hc2* line in *H-T* plane. For details and fitting curves, see text.

5. *Conclusion*

Superconductivity of the layered organic conductor, α–(BEDT-TTF)$_2$NH$_4$Hg(SCN)$_4$, was investigated by the in-plane and out-of-plane resistive and ac magnetic measurements in both a zero and dc fields. Through the in-plane resistive and high sensitive ac susceptibility measurements, the quasisuperconducting state was found in the temperature range of 1K-2.4K. Considering the two-dimensionality of the superconductivity in the present system, this phenomenon is suggested to have some relation to the Kosterlitz-Thouless behavior, which also shows nonlinerity in the I-V characteristics as was observed in some samples but with less reproducibility. Out-of-plane ac susceptibility gave the out-of-plane penetration depth, $\lambda_{\perp}(0)$, of 1.4mm, which is the largest among those of the organic superconductors. The anisotropy parameter deduced from resistivity and penetration depth amounts to the order of 10^3, which classifies this organic system to a class of extremely-anisotropic superconductors. Reflecting the large anisotropy and the large in-plane penetration depth, the vortex liquid state is considered to exist in the wide range of the mixed state. Indeed the region, where the vortices are mobile freely, were observed through both the in-plane and out-of-plane ac susceptibility measurements under fields below the H_{c2} line, which was determined by the specific heat measurements. The out-of-plane resistivity under fields gave the sample-independent characteristic line in the vortex liquid phase in the H-T plane, which is suggestive of the decoupling of the mobile pancake vortices. From the superconducting parameters obtained in the present study, the pancake vortices in this superconductor is found to be mainly coupled by the electromagnetic energy. Reflecting this feature, the

temperature dependence of both the inductive and the out-of-plane resistive transition under fields were qualitatively explained by the recent melting theory and the decoupling theory taking account of the electromagnetic coupling. As for the vortex lattice melting, it was quantitatively well explained with the reasonable values of superconducting parameters.

References

[1] J.G. Bednorz and K.A. Muller, Z.Phys. B**64**, 189 (1986)

[2] M. K. Wu, et al., Phys. Rev. Lett. **58**, 908 (1987)

[3] H. Maeda, et al., Jpn. J. Appl. Phys. **27**, L209 (1988)

[4] T. T. M. Palstra, et al., Phys. Rev. Lett. **61**, 1662 (1988)

[5] Y. Yamaguchi, et al., Physica C**228**, 141 (1994)

[6] H. Safar, et al., Phys. Rev. Lett. **69**, 824 (1992)

[7] W. K. Kwok, et al., Phys. Rev. Lett. **72**, 1092 (1994)

[8] S. Watauchi, et al., Physica C**259**, 373 (1996)

[9] D. Majer, et al., Phys. Rev. Lett. **75**, 1166 (1995)

[10] A. Shilling et al., Nature **382**, 791 (1996)

[11] A. Houghton, et al., Phys. Rev. B**40**, 6763 (1989)

[12] W.E. Lawrence and S. Doniach, in *Proceedings of 12th International Conference on Low Temperature Physics, Kyoto, 1970*, edited by E. Kanda

[13] M. Tinkham, *Introduction to Superconductivity, 1975*, McGraw-Hill, New York

[14] L. I. Glazman and A. E. Koshelev, Phys. Rev. B**43**, 2835 (1991) ; M. V. Feigel'man et al., Physica C **167**, 177 (1990)

[15] R. Ikeda, J. Phys. Soc. Jpn. **64**, 1683 (1995)

[16] T. Tamegai et al., Physica C **213**, 33 (1993)

[17] R. Cubitt et al., Nature (London) **365**, 407, (1993)

[18] S. L. Lee et al., Phys. Rev. Lett. **75**, 922 (1995)

[19] R. A. Doyle et al., Phys. Rev. Lett. **75**, 4520 (1995)

[20] In κ-ET, for $\xi_{//}$ (or $H_{c2//}$), J. E. Graebner et al., Phys. Rev. B**41**, 4808 (1990), for $\lambda_{//}$, [12] [13] [14] and for $\lambda_{\perp}$, [21] . In BSCCO, for $\xi_{//}$ (or $H_{c2//}$), B. Batlogg et al., Physica C **153-155**, 1062 (1988) ; A. S. Alexandrov et al., Phys. Rev. Lett. **76**, 983 (1996), for $\lambda_{//}$, D. R. Harshman et al Phys. Rev. Lett. **67**, 3152 (1991) ; T. Shibauchi et al., Physica C **203**, 315 (1992) and for $\lambda_{\perp}$, T. Jacobs et al., Phys. Rev. Lett. **75**, 4516 (1995)

[21] P. A. Mansky et al., Phys. Rev. B**50**, 15920 (1994)

[22] P.A. Mansky et al., Phys. Rev. Lett. **70**, 1323 (1993)

[23] H. H. Wang et al., Physica C **166**, 57 (1990)

[24] For α-ET, H. Mori et al., Synth. Met. **41-43**, 2013 (1991). For κ-ET, H. Urayama, et al., Chem. Lett. **1988**, 463 (1988); G. Saito et al., Synth. Met. A**331-340**, 27 (1988)

[25] M. Oshima et al., Chem. Lett. 1159 (1989)

[26] R. Bush et al., Phys. Rev. Lett. **69**, 522 (1992)

[27] S. Martin et al., Phys. Rev. Lett. **60**, 2194 (1988)

[28] K. Murata et al., Synth. Met. A**263-270**, 27 (1989)

[29] Y. Nakazawa et al., Phys. Rev. B**52**, 12890 (1995)

[30] K. Kanoda et al., Synth. Met. **55-57**, 2865 (1993)

[31] Y. Nakazawa et al., Synth. Met. **70,** 919 (1995)

[32] M. Lang et al., Phys. Rev. Lett. **69**, 1443 (1992)

[33] D. R. Harshman et al., Phys. Rev. Lett. **64**, 1293 (1990) ; Phys. Rev. B**49**, 12990 (1994)

[34] O. Klein et al., Phys. Rev. Lett. **66**, 655 (1991)

[35] S. Martin et al., Phys. Rev. Lett. **62**, 677 (1989)

[36] D. H. Kim et al., Phys. Rev. B**40**, 8834 (1989)

[37] Y. M. Wan et al., Phys. Rev. Lett. **71**, 157 (1993)

[38] K. Oshima et al., Synth. Met. A**419**, 27 (1988)

[39] private communication

[40] B. Andraka, et al., Phys. Rev. B**42** (1990) 9963

[41] A. E. Koshelev, Phys. Rev. Lett. **76,** 1340 (1996)

[42] G. Blatter et al., Phys. Rev. B**54**, 72 (1996)

[43] L. L. Deamen et al., Phys. Rev. B**47**, 11291 (1993)

[44] D.G. Steel et al., Phys. Rev, Lett. **71**, 161 (1993)

Acknowledgments

I would like to express my sincerest gratitude to Prof. K. Kanoda for his continuous interests, encouragement and discussions throughout the course of my doctoral program. Everything I have learned about physics during the past three years I owe it to him. He has also read all my manuscripts, of course, including this thesis and always give me constructive criticisms and enlightening advises.

I am deeply grateful to all the members of the Kanoda research group. Dr. Y. Nakazawa has told me many things. He has given me extensive knowledge about general experiments and physics. Mr. K. Miyagawa has helped me, whenever I have troubles. Secretary Miss. T. Iwatuki has given me kindness and encouragement. Dr. Kawamoto gave me the knowledge about organics and the organic-research world. And I am indebted to Dr. H. Sato for his helpful advises about transport measurements and research of superconductivity in the early stage of my doctoral course.

I had pleasure to enjoy the IMS-life with my colleagues. I would like to thank Mr. K. Hiraki and Mr. N. Takahashi for their encouragement and mental relief. All my friends have given me helps, supports and funs.

I would like to express my indebtedness to Prof. Y. Ishihara and Dr. H. Okamoto for their encouragement and discussions. I am deeply indebted to Prof. S. Naoe for giving me an opportunity for seeing the IMS.

Finally, I wish to thank my parents, brothers and their family for their incessant encouragement for many years.

Nov. 1996

Hiromi Taniguchi